Geometrically exact dynamics of cantilevered pipes conveying fluid

Hamed Farokhi[a], Mohammad Tavallaeinejad[b], Michael P. Païdoussis[b,*]

[a]*Department of Mechanical and Construction Engineering, Northumbria University, Newcastle upon Tyne NE1 8ST, UK*
[b]*Department of Mechanical Engineering, McGill University, Montréal, QC, Canada H3A 0C3*

Abstract

In this paper, the global dynamics of a hanging fluid conveying cantilevered pipe with a concentrated mass attached at the free end is investigated. The problem is of interest not only for engineering applications, but also because it displays interesting and often surprising dynamical behaviour. The widely used nonlinear models based on the transverse motion of the pipe are not able to accurately capture the dynamical behaviour of the system at very high flow velocities. Thus, a high-dimensional geometrically-exact model is developed for the first time, utilising Hamilton's principle together with the Galerkin modal decomposition technique. Extensive numerical simulations are conducted to investigate the influence of key system parameters. It is shown that at sufficiently high flow velocities past the first instability (Hopf bifurcation), the system undergoes multiple bifurcations with extremely large oscillation amplitudes and rotations, beyond the validity of third-order nonlinear models proposed to-date. In the presence of an additional tip mass, quasi-periodic and chaotic motions are observed; additionally, it is shown that for such cases an exact model is absolutely essential for capturing the pipe dynamics even at relatively small flow velocities beyond the first instability.

Keywords: Pipes conveying fluids; Nonlinear dynamics; Geometrically exact model; Chaos

1. Introduction

Real-world applications of pipes conveying fluid are numerous. They range from the small, such as micro and nano-tubes conveying fluid (Sadeghi-Goughari *et al.* 2020) and Coriolis type flow-meters (Zheng *et al.* 2016), to the very large, such as heat exchanger tubes, pipelines conveying liquid hydrocarbons (Mohmmed *et al.* 2020), as well as pipes used in ocean mining (Païdoussis & Luu 1985).

As demonstrated by Païdoussis & Li (1993), the generic system of a pipe conveying fluid has become a model problem in dynamics, on a par with the classical problem of a column subjected to an end-load, and indeed with a far wider repertoire. An abbreviated review of previous work is given here, focusing on cantilevered pipes conveying fluid, the subject of the present paper.

The first serious study of the system was made by Bourrières (1939), obtaining the basic equation of motion and reporting that the system loses stability by amplified oscillation (flutter) at sufficiently high flow velocities – also reporting on earlier observations by Brillouin, dating back to 1885. In the maelstrom of the Second World War, this study was effectively 'lost'.[1] The dynamics was therefore studied *ab initio* by Benjamin (1961*a*,*b*) in a seminal theoretical and experimental study, elucidating the fluid-structure energy transfer mechanisms underlying the dynamics and the generation of flutter. Detailed calculations,

*Corresponding author
Email address: michael.paidoussis@mcgill.ca (Michael P. Païdoussis)
[1]It was rediscovered in 1973; refer to Païdoussis & Issid (1974).

however, were confined to articulated models of the pipe. The equation of motion of the continuously flexible cantilevered system was solved for the first time by Païdoussis (1963), who also conducted experiments on a horizontal pipe conveying fluid, as reported in Gregory & Païdoussis (1966*a*,*b*).

It was found (Benjamin 1961*a*;Gregory & Païdoussis 1966*a*) that that the dynamics of the system is controlled by a dimensionless flow velocity, u, which is dependent on a single parameter, β, defined by

$$u = \left(\frac{M}{EI}\right)^{1/2} LU, \qquad \beta = \frac{M}{M+m}, \tag{1}$$

where M is the mass of the conveyed fluid per unit length with velocity U, EI is the flextural rigidity of the pipe, L its length and m its mass per unit length. The critical flow velocity for flutter, u_{cr}, increases with β discontinuously, exhibiting a number of 'jumps', shown much later to be associated with changes in modal content of the fluttering pipe (Semler *et al.* 1998). The interesting feature was demonstrated that, this being a non-conservative system, dissipation can be destabilizing.

Vertical systems were studied by Greenwald & Dugundji (1967) and Païdoussis (1970). The dynamics in this case is also dependent on the parameter

$$\gamma = \frac{M+m}{EI} gL^3, \tag{2}$$

where g is the acceleration due to gravity. More recently, in a very important study, Doaré & de Langre (2002*a*,*b*) showed that, for very long hanging pipes, the critical flow velocity does not diminish indefinitely with increasing length, but it reaches a plateau, as a result of gravity-induced effective 'rigidification' of the upper portion of the pipe.

Many variants of the basic system have been studied over the past 50 years: pipes with added masses, springs, dashpots and attached plates, pipes on elastic foundations, and so on, displaying a cornucopia of interesting and often unexpected dynamical behaviour , as reviewed in Païdoussis (2014). Also, the effects of a nonuniform velocity profile in the pipe (Guo *et al.* 2010), two-phase flow (Monette & Pettigrew 2004; Ebrahimi-Mamaghani *et al.* 2019), harmonically perturbed (pulsating) flow (Païdoussis & Issid 1974; Païdoussis & Sundararajan 1975), externally excited pipes (Sazesh & Shams 2019), and pipes with support imperfections (Kheiri 2020) have also been studied.

Finally, it was found, and demonstrated experimentally, that if the outlet at the free end is blocked and the fluid forced to exit radially rather than axially, flutter is suppressed unconditionally (Rinaldi & Païdoussis 2010).

In all the foregoing, the fluid flow is directed from the clamped towards the free end. The opposite flow configuration. usually referred to as 'a pipe aspirating fluid', has also been studied extensively for the following reason: for a long time, it could not unequivocally be decided whether the system develops flutter at sufficiently high flow velocity or not. It was finally concluded that it does, but the flutter is rather anaemic as compared to the fluid-discharging case; refer to Kuiper & Metrikine (2005), Païdoussis *et al.* (2005), and Païdoussis & Tétreault-Friend (2009).

In most of the foregoing, the analytical models are linear. However, there exists extensive literature on the nonlinear dynamics of the system. Thus, Bajaj *et al.* (1980) found that the Hopf bifurcation leading to flutter could be either subcritical or supercritical, depending on a friction-related parameter. Bajaj & Sethna (1984) found that flutter can be either planar (2-D) or circular (rotary, 3-D), depending on β in a disordered manner, and Modarres-Sadeghi *et al.* (2008) found that with increasing u the flutter motions could switch from 2-D to 3-D and *vice versa*.

Pipes with an inter-span spring support were studied by Païdoussis & Semler (1993), in particular 2-D motion in the vicinity of double degeneracy conditions, i.e. where static divergence and flutter coexist. Also, 3-D motions were studied by Steindl & Troger (1995), Wadham-Gagnon *et al.* (2007) and Païdoussis *et al.* (2007) finding a very intricate and rich dynamical behaviour

with increasing u, involving buckling, periodic and quasiperiodic flutter, oval and figure-of-eight oscillations, and chaotic motions.

A set of remarkable experiments by Copeland & Moon (1992) revealed that a pipe with an end-mass conveying fluid can display a very rich repertoire of dynamics as u is increased and γ varied: planar pendular and rotary motions, nutation, combined pendular and planar motions and chaos. This spurred further, theoretical and experimental studies, e.g. by Païdoussis & Semler (1998), Modarres-Sadeghi *et al.* (2007) and Ghayesh & Païdoussis (2010). In one bifurcation diagram, for example, the system went through the following sequence of states as u was increased: (i) planar periodic flutter; (ii) planar quasiperiodic oscillations; (iii) a frequency jump and return to periodic flutter; (iv) chaotic oscillations; (v) 3-D, planar period-1 and chaotic oscillations, sequentially; (vi) quasi-periodic oscillations. Some of these states were observed in the associated experiments.

The analytical models utilised in the studies discussed just above were third-order nonlinear models, even though the predicted oscillations were of large amplitude – large enough to render some of the results questionable. Fifth-order models would be quite unwieldy and more prone to numerical inaccuracies. The large-amplitude response of beams has been examined before, utilising finite element approaches together with exact displacement formulations by Pai (2014); Simo & Vu-Quoc (1988). A finite-volume momentum-based nonlinear approach has also been recently used for large-amplitude dynamical analysis of pipes conveying fluid in Tang & Sweetman (2021); the authors used piecewise linearisation in the time-domain to obtain the dynamical response of the system. The present study proposes a geometrically exact analytical model based on the beam centreline rotation, which circumvents the difficulties associated with large-amplitude dynamics of the pipe.

The review of previous work, leading to the *raison d'être* of the present paper, is quite long, but it is hoped interesting; yet, it is not exhaustive. Extensive reviews of previous work may be found in Ibrahim (2010, 2011), and Païdoussis (2014).

The main objective of this paper is to explore the global dynamics of a hanging fluid conveying cantilevered pipe with a concentrated mass attached at the free end, with special focus on high flow velocities. For this purpose, the classical nonlinear model of Païdoussis & Semler (1998) is revisited, relaxing the major assumption of finite deflection of the pipe. Thus, an analytical, high-dimensional, geometrically-exact model is developed in Section 2 for cantilevered pipes undergoing motions of extremely large amplitudes and rotations. Due to significant challenges encountered when relaxing the finite deflection assumption, a high-dimensional model has not been reported heretofore. Such high-dimensional discretisations are, however, essential to predict the rich dynamics of the system at high flow velocities, as discussed in Section 3. Extensive numerical results are obtained for the first time for such a high-dimensional exact model in Section 4 for different system parameters. Finally, the summary of findings is presented in Section 5.

2. Analytical models

In this section, a detailed derivation of the geometrically exact nonlinear model for a hanging cantilevered pipe is undertaken with the assumption of an inextensible centreline. The derivation to be presented here, so far as the structure of the system is concerned, is similar in spirit and procedure to that in Tavallaeinejad *et al.* (2018, 2020).

2.1. Basic assumptions and concepts

The system under consideration consists of a flexible pipe of mass per unit length m, flexural rigidity El, length L, material damping α, and cross-sectional area A, discharging an incompressible fluid of mass per unit length M flowing with a constant mean velocity U; a concentrated mass m_e is assumed to be attached at the free end (see Fig. 1). The XY coordinate system is

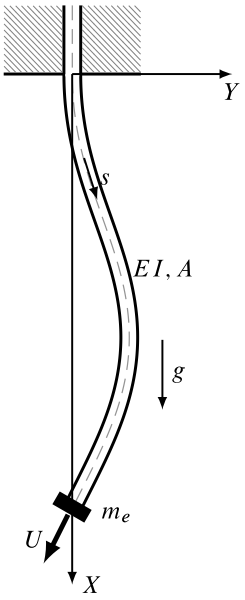

Figure 1: Schematic of cantilevered pipe conveying flow with added end-mass.

associated with the undeformed state of the pipe. The X-axis coincides with the direction of gravity and the pipe is assumed to oscillate only in the XY plane. Thus, the pipe undergoes two motions: $w(s,t)$, in the transverse direction and $v(s,t)$, in the longitudinal direction.

For the derivation procedure, the xy coordinate system is used which relates to the original XY coordinate system by: $x = v + X$ and $y = w + Y$. The curvilinear coordinate s denotes the distance of an element of the pipe from the clamped end.

Although deflections of the pipe may be extremely large, the strains remain small; hence, the pipe centreline is assumed inextensible; i.e., $(\partial_s x(s,t))^2 + (\partial_s y(s,t))^2 = 1$. As such, the centreline slope, $\theta(s,t)$, and curvature, $\kappa(s,t)$, are related to the longitudinal, $v(s,t)$, and transverse, $w(s,t)$, motions of the pipe through

$$\sin\theta(s,t) = \partial_s y(s,t) = \partial_s w(s,t), \quad \cos\theta(s,t) = \partial_s x(s,t) = 1 + \partial_s v(s,t), \quad \kappa(s,t) = \partial_s \theta(s,t). \tag{3}$$

Note that the operator $\partial_s \equiv \partial/\partial s$ denotes the first derivative with respect to variable s. Hence, the displacement and the velocity components of an element can be formulated as

$$\begin{aligned} y(s,t) &= \int_0^s \sin\theta(s^*,t)\,\mathrm{d}s^*, & x(s,t) &= \int_0^s \cos\theta(s^*,t)\,\mathrm{d}s^*, \\ \partial_t y(s,t) &= \int_0^s \partial_t\theta(s^*,t)\cos\theta(s^*,t)\,\mathrm{d}s^*, & \partial_t x(s,t) &= -\int_0^s \partial_t\theta(s^*,t)\sin\theta(s^*,t)\,\mathrm{d}s^*. \end{aligned} \tag{4}$$

2.2. The energy method

In this paper, a Hamiltonian framework is adopted. The extended Hamilton's principle for an open system may be expressed as

$$\delta\int_{t_1}^{t_2} \big(\mathcal{T}(t) - \mathcal{V}(t)\big)\,\mathrm{d}t + \int_{t_1}^{t_2} \delta\big(\mathcal{W}_\mathrm{f}(t) + \mathcal{W}_\mathrm{d}(t)\big)\,\mathrm{d}t = 0, \tag{5}$$

with $\mathcal{T}(t)$ and $\mathcal{V}(t)$ denoting the kinetic and potential energies of the system, respectively, and $\delta\mathcal{W}_\mathrm{f}$ and $\delta\mathcal{W}_\mathrm{d}$ the virtual work by the fluid forces and damping, respectively; here δ denotes the variational operator.

Considering the velocity of an infinitesimal element of the cantilevered pipe, $\mathbf{V}_\mathrm{p} = \partial_t x(s,t)\mathbf{i} + \partial_t y(s,t)\mathbf{j}$, and the fluid,

$\mathbf{V}_{\mathrm{f}} = (\partial_t x(s,t) + U\cos\theta(s,t))\mathbf{i} + (\partial_t y(s,t) + U\sin\theta(s,t))\mathbf{j}$, the total kinetic energy can be written as

$$\begin{aligned}\mathcal{T}(t) = &\frac{1}{2}\int_0^L (M + m(s))\left((\partial_t x)^2 + (\partial_t y)^2\right)\mathrm{d}s + \frac{1}{2}M\int_0^L U^2\mathrm{d}s \\ &+ \frac{1}{2}M\int_0^L \Big(2U\partial_t x\cos\theta + 2U\partial_t y\sin\theta\Big)\mathrm{d}s,\end{aligned} \tag{6}$$

in which $m(s) = m + m_e\delta_{\mathrm{D}}\left(x(s,t) - L\right)$, where δ_{D} denotes the Dirac delta function.

The potential energy of the pipe comprises strain and gravitational energy components. An exact form of the variation of the potential energy, in the case of large deflections and small strains may be formulated as

$$\begin{aligned}\delta\mathcal{V}(t) =&EI\int_0^L \partial_s\theta(s,t)\partial_s(\delta\theta(s,t))\,\mathrm{d}s - (M+m)g\int_0^L \delta x(s,t)\,\mathrm{d}s \\ &- m_e g\int_0^L \delta_{\mathrm{D}}\left(x(s,t) - L\right)\delta x(s,t)\,\mathrm{d}s.\end{aligned} \tag{7}$$

Various models may be used for the structural damping. In this paper, the Kelvin-Voigt structural damping is adopted. Thus, the virtual work associated with the viscous component of the axial stress may be formulated as

$$\delta\mathcal{W}_{\mathrm{d}}(t) = -\alpha I\int_0^L \partial_s(\partial_t\theta(s,t))\partial_s(\delta\theta(s,t))\,\mathrm{d}s. \tag{8}$$

Finally, the virtual work done by nonconservative fluid forces associated with the fluid exiting the pipe can be expressed as

$$\int_{t_1}^{t_2}\delta\mathcal{W}_{\mathrm{f}}(t)\,\mathrm{d}t = -MU\int_{t_1}^{t_2}\Big[\big(\partial_t x(L,t) + U\partial_s x(s=L,t)\big)\delta x(L,t) + \big(\partial_t y(L,t) + U\partial_s y(s=L,t)\big)\delta y(L,t)\Big]\,\mathrm{d}t. \tag{9}$$

2.3. Geometrically-exact model

Substituting Eqs. (6)-(9) into the Hamilton's principle given in Eq. (5), performing some mathematical manipulations, and employing the relationships in Eq. (4) yields the exact model governing the cross-section rotation of the fluid-conveying cantilevered pipe. Utilising the following dimensionless parameters:

$$\begin{aligned}&\xi = \frac{s}{L},\quad \eta = w/L,\quad \zeta = v/L,\quad \tau = \frac{t}{T},\quad \gamma = \frac{m+M}{EI}gL^3,\quad \beta = \frac{M}{m+M}, \\ &\Gamma = \frac{m_e}{(m+M)L},\quad \alpha_s = \frac{\alpha}{ET},\quad m(\xi) = 1 + \Gamma\delta_{\mathrm{D}}(\xi - 1),\quad u = \left(\frac{M}{EI}\right)^{1/2}LU,\end{aligned} \tag{10}$$

where $T = L^2\left[(m+M)/EI\right]^{\frac{1}{2}}$, the dimensionless form of the geometrically-exact equation of a pipe conveying fluid is

$$\begin{aligned}&\cos\theta(\xi,\tau)\int_\xi^1\Bigg\{m(\tilde{\xi})\int_0^{\tilde{\xi}}\Big[\partial_{\tau\tau}\theta(\xi^*,\tau)\cos\theta(\xi^*,\tau) - (\partial_\tau\theta(\xi^*,\tau))^2\sin\theta(\xi^*,\tau)\Big]\,\mathrm{d}\xi^* \\ &+ 2u\sqrt{\beta}\partial_\tau\theta(\tilde{\xi},\tau)\cos\theta(\tilde{\xi},\tau) + u^2\partial_{\tilde{\xi}}\theta(\tilde{\xi},\tau)\cos\theta(\tilde{\xi},\tau)\Bigg\}\mathrm{d}\tilde{\xi} \\ &+ \sin\theta(\xi,\tau)\int_\xi^1\Bigg\{m(\tilde{\xi})\int_0^{\tilde{\xi}}\Big[\partial_{\tau\tau}\theta(\xi^*,\tau)\sin\theta(\xi^*,\tau) + (\partial_\tau\theta(\xi^*,\tau))^2\cos\theta(\xi^*,\tau)\Big]\,\mathrm{d}\xi^* \\ &+ 2u\sqrt{\beta}\partial_\tau\theta(\tilde{\xi},\tau)\sin\theta(\tilde{\xi},\tau) + u^2\partial_{\tilde{\xi}}\theta(\tilde{\xi},\tau)\sin\theta(\tilde{\xi},\tau) + m(\tilde{\xi})\gamma\Bigg\}\mathrm{d}\tilde{\xi} \\ &- \partial_{\xi\xi}\theta(\xi,\tau) - \alpha_s\partial_{\xi\xi}\left(\partial_\tau\theta(\xi,\tau)\right) = 0.\end{aligned} \tag{11}$$

2.4. *Nonlinear third-order model of Païdoussis & Semler (1998)*

The equation of motion given in Eq. (11) can be recast in terms of the transverse displacement of the pipe via truncating the nonlinear exact terms while retaining terms up to third order. One can obtain the equivalent third-order nonlinear equation of motion as

$$\begin{aligned}
&m(\xi)\partial_{\tau\tau}\eta + (1+\alpha_s\partial_\tau)\,\partial_{\xi\xi\xi\xi}\eta + 2\sqrt{\beta}u\partial_{\xi\tau}\eta + u^2\partial_{\xi\xi}\eta + 4\partial_\xi\eta\,\partial_{\xi\xi}\eta\,\partial_{\xi\xi\xi}\eta + (\partial_{\xi\xi}\eta)^3 + \partial_{\xi\xi\xi\xi}\eta(\partial_\xi\eta)^2 \\
&\quad + \alpha_s\frac{\partial}{\partial\xi}\Big((\partial_\xi\eta)^2\partial_{\xi\xi\xi\tau}\eta + \partial_\xi\eta\,\partial_{\xi\tau}\eta\,\partial_{\xi\xi\xi}\eta + \partial_{\xi\tau}\eta\,(\partial_{\xi\xi}\eta)^2 + 2\partial_\xi\eta\,\partial_{\xi\xi}\eta\,\partial_{\xi\xi\tau}\eta\Big) \\
&\quad + 2u\sqrt{\beta}\partial_{\xi\tau}\eta(\partial_\xi\eta)^2 + u^2\partial_{\xi\xi}\eta(\partial_\xi\eta)^2 + \gamma m(\xi)\partial_\xi\eta\Big(1+\frac{1}{2}(\partial_\xi\eta)^2\Big) \\
&\quad + m(\xi)\partial_\xi\eta\int_0^\xi\frac{\partial}{\partial\tau}\Big(\partial_{\tilde\xi\tau}\eta(\tilde\xi,\tau)\partial_{\tilde\xi}\eta(\tilde\xi,\tau)\Big)\mathrm{d}\tilde\xi - \partial_{\xi\xi}\eta\int_\xi^1 m(\tilde\xi)\int_0^{\tilde\xi}\frac{\partial}{\partial\tau}\Big(\partial_{\xi^*\tau}\eta(\xi^*,\tau)\partial_{\xi^*}\eta(\xi^*,\tau)\Big)\mathrm{d}\xi^*\,\mathrm{d}\tilde\xi \\
&\quad - \partial_{\xi\xi}\eta\int_\xi^1\Big(2u\sqrt{\beta}\partial_{\tilde\xi\tau}\eta(\tilde\xi,\tau) + u^2\partial_{\tilde\xi\tilde\xi}\eta(\tilde\xi,\tau)\Big)\partial_{\tilde\xi}\eta\,\mathrm{d}\tilde\xi - \Big(\partial_{\xi\xi}\eta + \frac{3}{2}(\partial_\xi\eta)^2\partial_{\xi\xi}\eta\Big)\int_\xi^1\gamma m(\tilde\xi)\mathrm{d}\tilde\xi.
\end{aligned} \tag{12}$$

The above equation of motion is identical to the third-order model of Païdoussis & Semler (1998) with the the only difference being in the damping term, with the current model being of Kelvin-Voigt type rather than a linear viscous one.

2.5. *Discretisation and solution techniques*

The nonlinear integro-partial differential models given in Eq. (11) and Eq. (12) are first discretised in space via a Galerkin technique.

As for Eq. (12), a linear combination of suitable admissible functions, $\phi_j(\xi)$, is selected to discretise the transverse motion: $\eta(\xi,\tau) = \sum_{j=1}^{M}\phi_j(\xi)q_j(\tau)$, with $q_j(\tau)$ denoting the unknown time-dependent generalised coordinates of transverse motion, and $\phi_j(\xi)$ being the jth eigenfunction of a linear cantilever beam[2].

In the proposed exact model, i.e. Eq. (11), the admissible functions $\Theta_j(\xi) = \partial_\xi\phi_j(\xi)/\beta_j$ (where β_j is the jth root of the transcendental equation $1+\cosh(\beta)\cos(\beta)=0$) are used to approximate the rotation of the pipe $\theta(\xi,\tau)$ as:

$$\theta(\xi,\tau) = \sum_{j=1}^{M}\Theta_j(\xi)p_j(\tau), \tag{13}$$

where $p_j(\tau)$ represents the unknown time-dependent generalised coordinates of centreline rotation.

In this study, the lowest 10 modes are retained in the series expansions for both exact and truncated models, i.e. $M=10$. The resultant 10-degree-of-freedom (dof) second-order nonlinear ordinary differential equations (ODEs) are then recast in a system of 20-dof first-order ODEs. The subsequent set of ODEs is solved using a pseudo-arclength continuation technique resulting in the bifurcation diagrams of the system. The Gear backward differentiation formula (BDF) is also used to obtain the bifurcation diagrams of Poincaré sections, as well as the time histories and phase-plane diagrams of oscillation. It should be noted that the high-dimensional discretisation of the proposed exact model is extremely challenging (this being the first time) because, unlike the truncated model, for the exact model the spatial integrations cannot be completed in closed-form and need to be performed numerically while keeping sufficient terms to ensure converged results. More specifically, considering the first line in Eq. (11), the terms under the integral $\int_0^{\tilde\xi}$ are also under another integral $\int_\xi^1$, and after application of the Galerkin

[2]Considering the large amplitude deformations of the pipe, the hyperbolic beam modes utilised in this paper, which represent the real motion of the beam obtained from a linear analysis, offer much better accuracy compared to polynomial functions. In particular, the polynomial functions lose accuracy rapidly in higher-order spatial differentiations.

technique will go under yet another integral $\int_0^1$; assuming N terms to approximate each integral via a numerical integration algorithm will lead to N^3 terms just for one of the triple integrals. Hence, this process leads to an extremely large set of discretised equations, but ensures accurate results.

Unless otherwise stated, the following values are considered throughout this study: $\beta = 0.142$ and $\gamma = 18.9$ as in Païdoussis & Semler (1998) based on the physical system studied therein; additionally, the dimensionless material viscosity α_s is set to 0.0018, which for small-amplitude oscillations is equivalent to the linear damping coefficient used for the 2nd transverse mode in Païdoussis & Semler (1998).

3. Convergence analysis and comparison to 3rd-order model

In this section, a detailed convergence test is conducted to highlight the significance of high-dimensional discretisation. Additionally, comparisons between the exact and the truncated nonlinear 3rd-order models are performed to show the limitations of the latter.

For the convergence analysis, several discretised models of the geometrically exact model are constructed, i.e. the 2-, 3-, 4-, 8-, and 10-dof ones. The bifurcation diagrams of the fluid-conveying cantilevered pipe are then constructed for all these discretised models, for three cases. Figure 2 shows the results of the convergence analysis for (a) $\Gamma = 0$, (b) $\Gamma = 0.10$, and (c) $\Gamma = 3.0$. As seen in Fig. 2(a), employing either 2- or 3-dof models leads to inaccurate predictions; additionally, the 4-dof model works well only for relatively low flow velocities, and it becomes inaccurate at relatively large flow velocities. The 8- and 10-dof models, on the other hand, predict almost identical responses, indicating convergence. A similar scenario is observed for the cases with $\Gamma = 0.10$ and 3.0; however, in these cases, the inaccuracies of the low-dimensional models (i.e. 2-, 3-, and 4-dof models) become more pronounced even at relatively small flow velocities. The comprehensive convergence analysis conducted in Fig. 2 shows that it is essential to retain at least 8 modes in the discretisation procedure to ensure converged results, up to $u \simeq 15$; it should be noted that the present study utilises a 10-dof model to ensure converged results for different values of the tip mass ratio even at large flow velocities.

Next, a comparison between the prediction of the proposed exact model and that of the third-order nonlinear model is conducted to further highlight the importance of utilising an exact model for investigating the behaviour of a fluid-conveying cantilevered pipe. First, it should be mentioned that, similarly to the exact model, a 10-dof discretisation is used for the 3rd-order nonlinear model, which is sufficient for obtaining converged results (determined via another convergence analysis on the 3rd-order model). The comparisons between the results obtained via the exact and 3rd-order models are shown in Fig. 3 for different values of Γ, to better highlight the differences between the two models.

It is seen in Fig. 3(a) that for $\Gamma = 0$, the difference in the transverse oscillation amplitude predicted by the two models becomes significant even at slightly higher flow velocities beyond the critical value. In particular, the 3rd-order model predicts the transverse amplitude with almost 20% error at $u = 8.74$; additionally, the 3rd-order model predicts unstable periodic response in the approximate u range of $[13\ 17]$, which is not the case according to the exact model. The difference between the two models becomes even more pronounced when $\Gamma = 0.10$ and 0.15 as shown in Fig. 3(b) and (c), respectively. More specifically, the error of 3rd-order model at $u = 7.30$ exceeds 37% when $\Gamma = 0.10$ and 54% when $\Gamma = 0.15$. More importantly, the 3rd-order model completely diverges at flow velocities larger than 13 for these two cases. A final comparison is made in Fig. 3(d) for the case with $\Gamma = 3.0$; as seen, the 3rd-order model quickly diverges almost immediately beyond u_{cr}. This comprehensive comparison between the proposed geometrically exact model and the 3rd-order nonlinear model

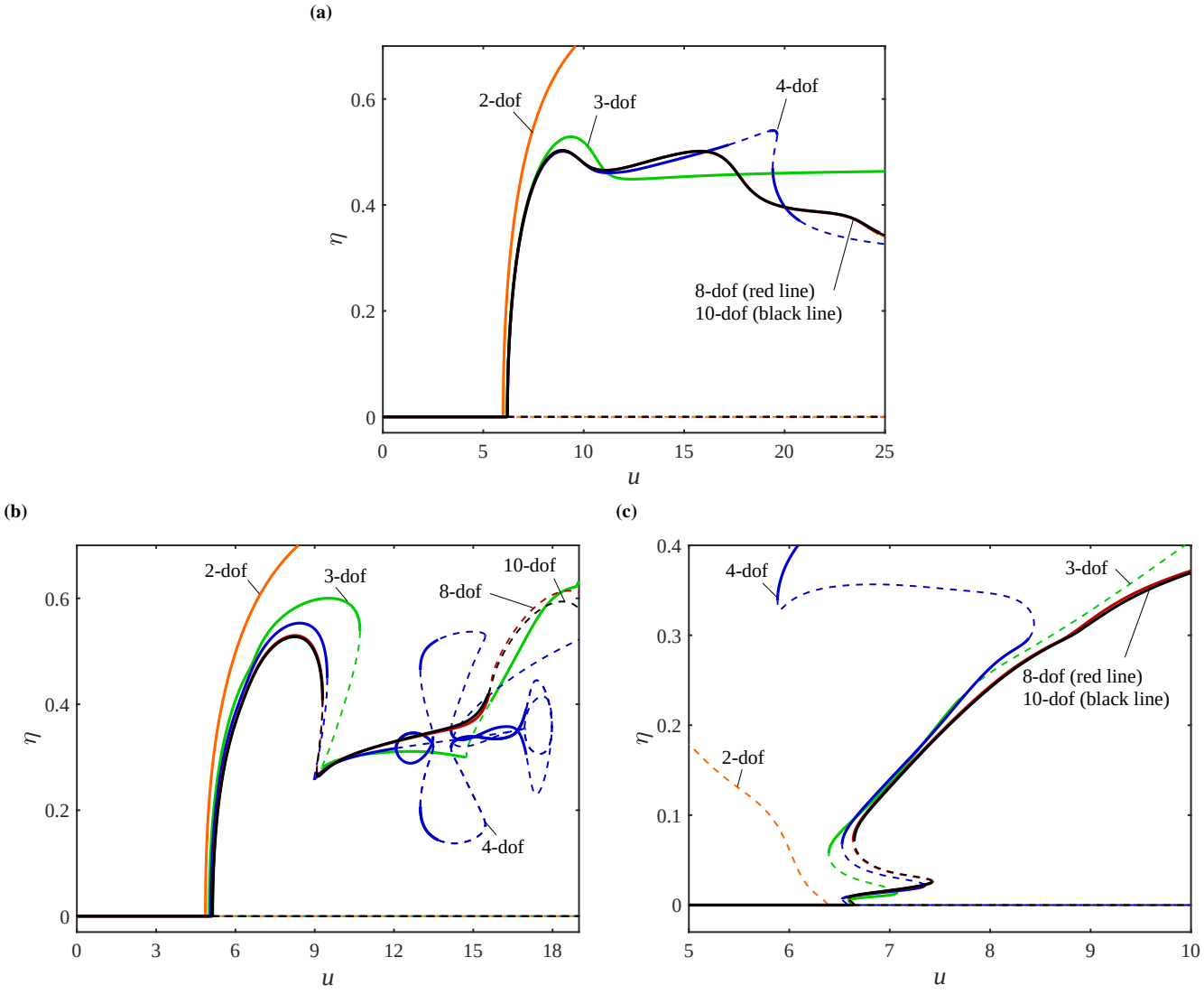

Figure 2: Convergence analysis of the proposed geometrically exact model showing the maximum transverse tip displacement for (a) $\Gamma = 0$, (b) $\Gamma = 0.10$, and (c) $\Gamma = 3.00$; $\beta = 0.142$ and $\gamma = 18.9$ for all cases.

demonstrates the necessity of utilising an exact model for predicting the post-critical dynamics of fluid-conveying cantilevered pipes accurately.

Furthermore, a comparison is made in Fig. 4 between the bifurcation diagram of a fluid-conveying pipe obtained by Païdoussis & Semler (1998) using a third-order model and that obtained via the proposed 10-dof exact model as well as the 10-dof 3rd-order model developed in this study. As seen, the response obtained by the 10-dof 3rd-order model used in this study almost matches that obtained by Païdoussis and Semler using a 4-dof third-order model, hence verifying the 3rd-order model utilised in this study. The exact model, on the other hand, predicts a generally smaller amplitude of oscillation for the flow range examined.

4. Results and discussion

In this section, the nonlinear aspects of the system dynamics, such as limit-cycle amplitudes and frequencies, as well as the transition between various dynamical states, are studied numerically. This is done via constructing bifurcation diagrams as well

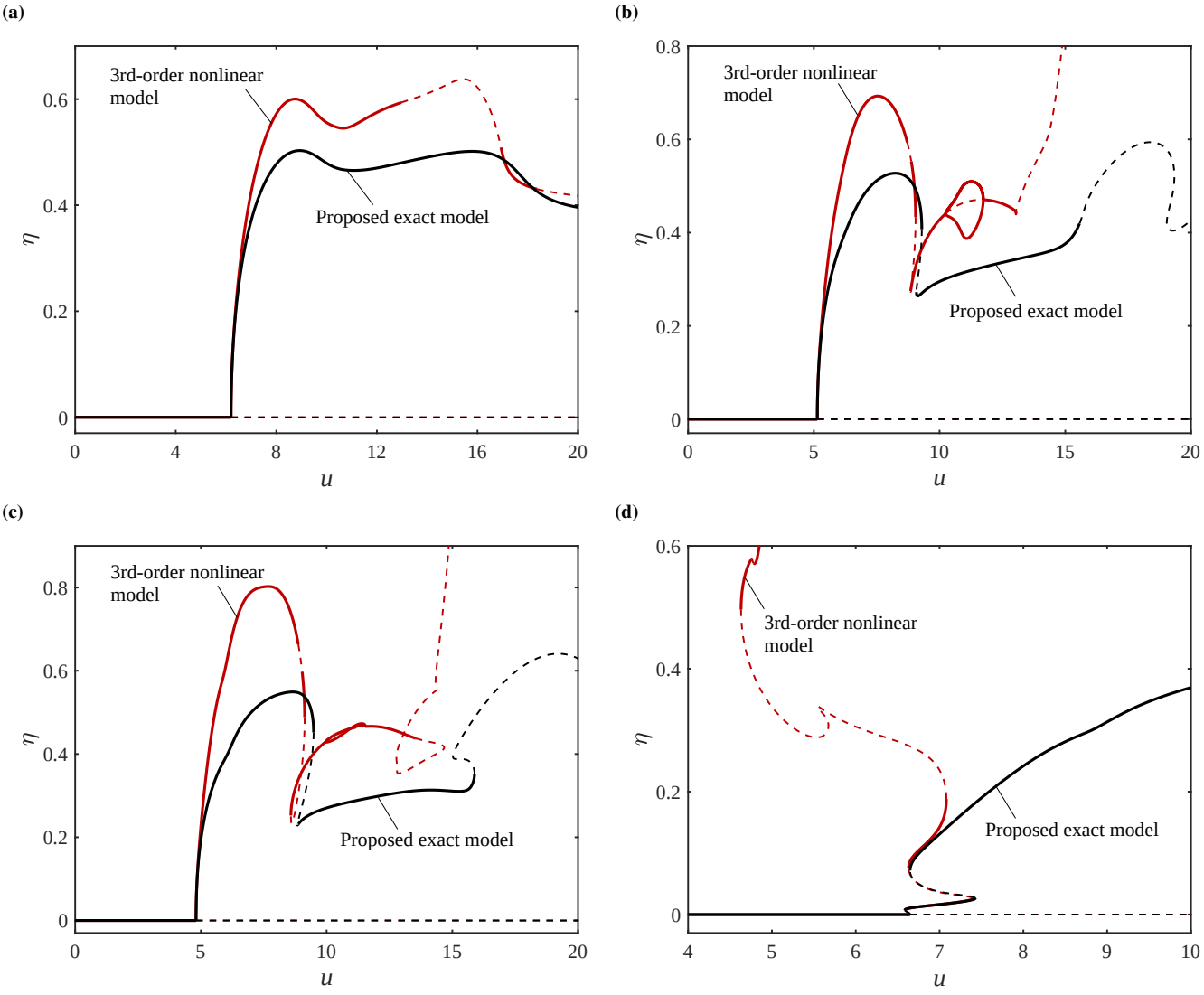

Figure 3: Comparison between the maximum transverse tip displacement obtained via the proposed geometrically exact model (10-dof) and that obtained via the third-order nonlinear model (10-dof) for (a) $\Gamma = 0$, (b) $\Gamma = 0.10$, (c) $\Gamma = 0.15$, and (d) $\Gamma = 3.00$; $\beta = 0.142$ and $\gamma = 18.9$ for all cases.

as shapes of pipe oscillations.

4.1. Exact pipe behaviour at relatively large flow velocities

Figure 5 shows the large-amplitude exact dynamic response of the fluid-conveying cantilevered pipe in the flow velocity range of $[0\ 25]$; the bifurcation diagrams are shown for (a) tip slope, (b) the dimensionless angular frequency of limit cycles (i.e. Ω, which is related to its dimensional counterpart ω via $\Omega = \omega T$), (c) tip dimensionless transverse displacement η, and (d) tip dimensionless axial displacement ζ. Figure 6 shows the detailed planar motion of the pipe at different flow velocities; it should be noted that in Fig. 6, X and Y denote the dimensionless (with respect to L) undeformed coordinates.

Increasing the flow velocity from zero, the system loses stability via a Hopf bifurcation at $u_{cr} = 6.20$; the cantilevered pipe starts oscillating in a plane, generally with a second cantilevered beam-mode shape (see Fig. 6(a)), with a dimensionless frequency of $\Omega_{cr} = 16.05$. This well-known phenomenon has been reported in theoretical and experimental studies previously by many researchers (Païdoussis 1963,1970;Païdoussis & Semler 1998).

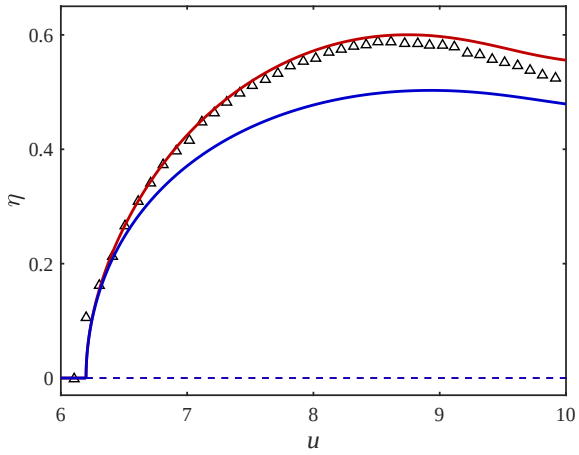

Figure 4: Bifurcation diagrams for $\beta = 0.142$, $\Gamma = 0$ and $\gamma = 18.9$; maximum transverse tip displacement of the pipe over a cycle of steady-state oscillation. [▬] Proposed exact model, [▬] 10-dof 3rd-order nonlinear model, [△] results obtained by Païdoussis & Semler (1998) using a 4-dof 3rd-order nonlinear model.

An interesting aspect of the pipe behaviour, as seen in Fig. 5, is that the tip transverse displacement magnitude reaches a maximum of 0.503 at $u = 8.93$; as the flow velocity is increased further, the tip transverse deflection is initially decreased and then increased until reaching a maximum of 0.501 at $u = 15.79$, and then decreases again. This is accompanied by the change in the dominant mode of oscillations and stronger contribution of higher modes in the response of the system (note the steady increase of oscillation frequency with flow velocity shown in Fig. 5(b)). This is also seen in sub-figures 6(a)-(f), where the tip transverse oscillation amplitude is initially increased as the flow velocity is increased, and then decreased with further increase of the flow velocity. It should be noted that the pipe displays stable periodic oscillations up to $u = 24.76$, where a torus bifurcation occurs and the motion becomes non-periodic.

Additionally, it is seen in Fig. 5 that a cantilevered fluid-conveying pipe undergoes extremely large rotations at relatively large flow velocities. In fact, it is noticed that for $u > 12.50$, the tip slope becomes larger than $\pi/2$; this is also visible in sub-figures 6(e) and (f). This is important in the sense that a nonlinear truncated third-order model *is not* capable of capturing such oscillation amplitudes accurately, due to its inherent third-order limitation which leads to significant error at relatively large tip angles (as further explained in Section 3), thus highlighting the significance of employing a geometrically exact model capable of capturing such large slopes reliably.

Figure 7 shows the effect of β on the global dynamics of the system. The Hopf bifurcation materialises at higher flow velocities with increasing β, while the amplitude decreases as a result of a change in the modal shape of the oscillations, as shown in Fig. 7(a). This is made clearer in Fig. 7(b), showing that the oscillation frequencies steadily increase with u and β. Additionally, in all three cases, the tip slope exceeds $\pi/2$ at high flow velocities. These observations indicate that the exact model, spatially discretised with a higher number of modes, is essential to adequately represent the dynamics of the system as β and u are increased. It is worth noting that the parameter β, being the coefficient of the Coriolis term in the nondimensional equation of motion, has a stabilising effect, thus causing u_{cr} to increase with increasing β. However, if this is looked upon from a *dimensional* analysis perspective, a higher β corresponds to a higher mass of fluid flow, which should lead to lower critical flow velocities; this indeed is the case: the dimensional critical flow velocities decrease with increasing β. Hence, care should be taken when discussing the variation of critical flow velocity with β.

The effect of the gravity parameter, γ, is investigated employing the geometrically exact model and the results are shown in Fig. 8. Since the pipe is hanging, a larger value of γ leads to increased tension in the pipe which in turn stabilizes the system and leads to a larger critical flow velocity. It is interesting to note that the difference between the amplitudes of oscillation for different values of γ becomes less significant at relatively large flow velocities.

4.2. Tip mass effect

In this section, the effect of the tip mass on the dynamics of the fluid-conveying cantilevered pipe is investigated. Two ranges of tip mass ratio parameter Γ are considered, i.e., a range of relatively small values: $\Gamma = 0.03$, 0.05, 0.10, and 0.15, as well as a range of relatively large values: $\Gamma = 1.0$, 2.0, and 3.0.

Figure 9 shows the bifurcation diagrams for the fluid-conveying cantilevered pipe for the small values of Γ. The corresponding diagrams for the dimensionless angular frequency of limit cycles for each value of Γ is depicted in Fig. 10. Finally, the pipe

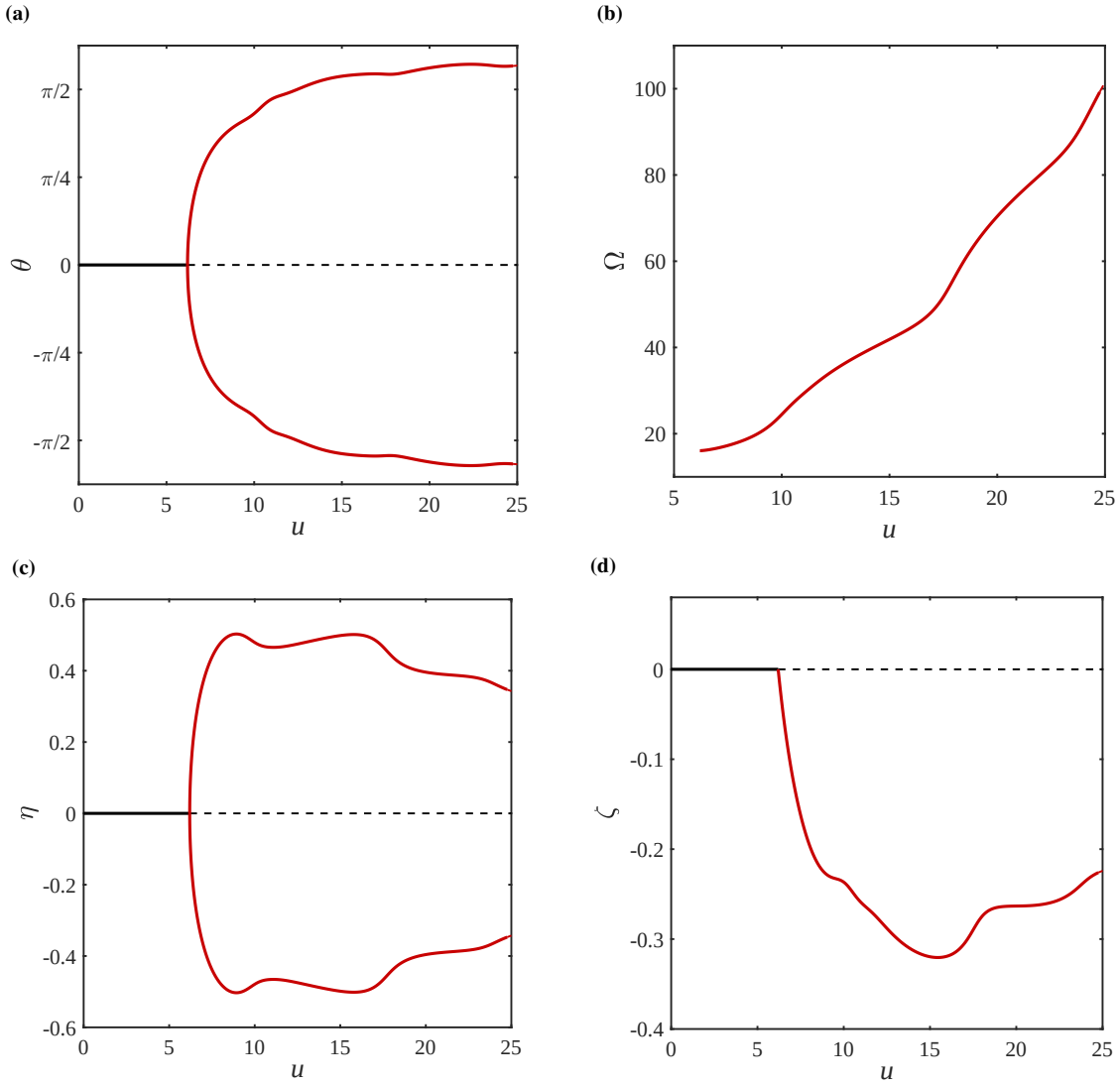

Figure 5: Bifurcation diagrams for $\beta = 0.142$, $\Gamma = 0$ and $\gamma = 18.9$. (a) Maximum/minimum values of the tip slope of the pipe over a cycle of steady-state oscillation. (b) Dimensionless angular frequency of oscillations. (c) Maximum/minimum values of the tip transverse motion and (d) the corresponding longitudinal motion over a cycle of steady-state oscillation. [▬] Stable static solution, [▪▪▪] unstable static solution, [▬] stable periodic solution.

motion at different flow velocities for the case $\Gamma = 0.10$ is shown in Fig. 11.

As seen in Fig. 9, in all cases, with increasing the flow velocity above the onset of flutter, the oscillation amplitude first increases and reaches an initial maximum in the range of $8.20 < u < 8.50$, and then undergoes a sharp reduction. More specifically, for the lightest tip mass with $\Gamma = 0.03$ (Figs. 9(a) and (b)), as the flow velocity is increased past the Hopf bifurcation, the pipe starts to oscillate and the amplitude of oscillation grows rapidly with increasing flow velocity. Various bifurcation types appear at $u > 15$, namely saddle-node and torus. The dimensionless frequency of oscillation for this case is shown in Fig. 10(a), showing that it generally increases with increasing flow velocity. The sharp increase in the frequency of oscillations in the vicinity of $u = 17$ is associated with the change in the mode of oscillations, thus resulting in a reduction in the transverse motion amplitude.

The dynamical behaviour of the pipe with $\Gamma = 0.05$ (Figs. 9(c) and (d)) is more sophisticated. For this case, branch points occur at $u < 15$, giving rise to a complex solution branch which itself includes saddle-node and torus bifurcations. The frequency of the dynamic response, as shown in Fig. 10(b), increases up to the first branch point; it is seen that the oscillation frequency of the bifurcated solution branch is smaller than that of the main branch. As the flow velocity is increased further, the oscillation frequency jumps to a larger value, indicating increased contribution of higher modes.

As Γ is increased to 0.10, the branch points disappear and the pipe displays generally simpler dynamics. The qualitative dynamical behaviour of the pipe with $\Gamma = 0.15$ is quite similar to that of the pipe with $\Gamma = 0.10$ with more substantial changes

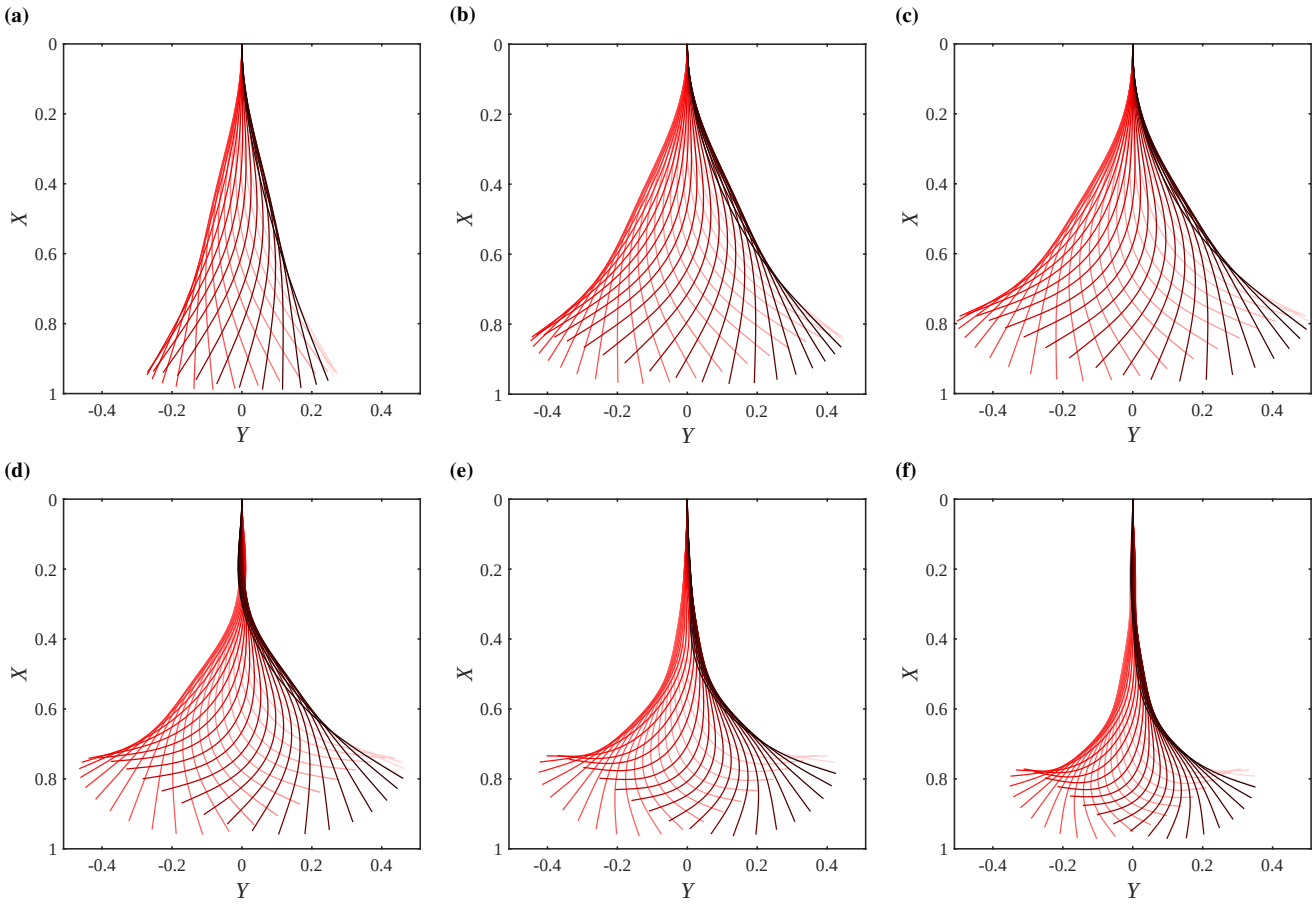

Figure 6: Shapes of the oscillating pipe; (a) $u = 6.60$, (b) $u = 7.65$, (c) $u = 8.94$, (d) $u = 11.10$, (e) $u = 18.40$, and (f) $u = 24.51$, showing that the tip angle exceeds $\pi/2$.

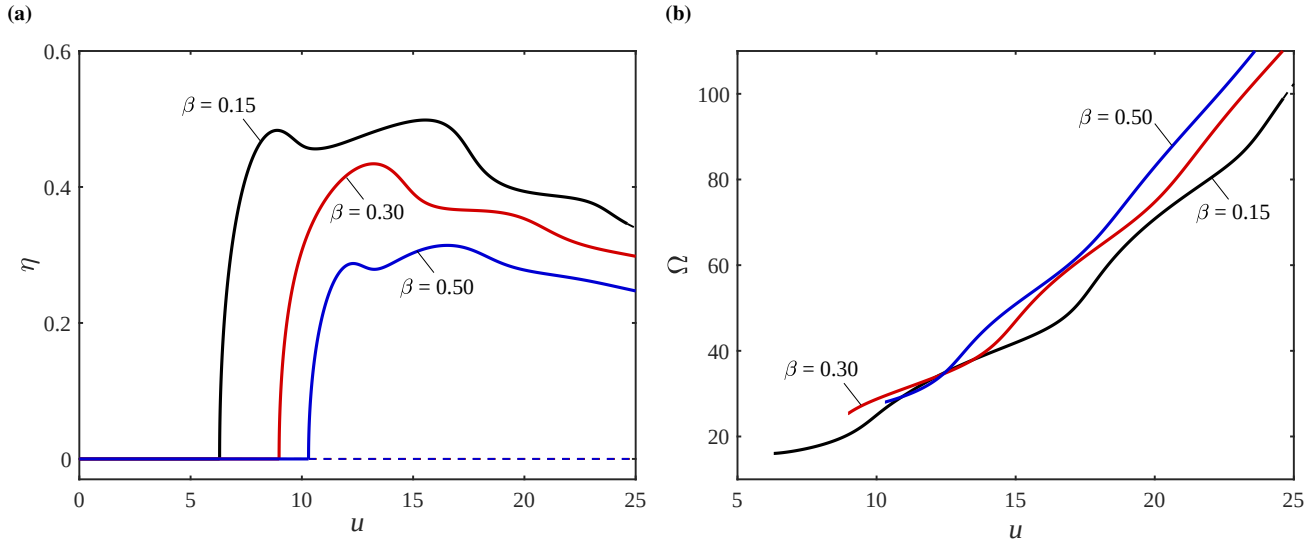

Figure 7: Bifurcation diagrams showing (a) the maximum (positive) transverse tip displacement and (b) the frequency of the transverse oscillation, obtained for a system with $\gamma = 18.9$, $\Gamma = 0$ and various values of β.

in the amplitude of oscillations with varying u. Moreover, the pipe in these two cases displays two saddle-node bifurcations and a torus bifurcation, but no branch point, which leads to slightly simpler dynamics compared to the previous cases. The oscillation frequency of the pipe for this case is illustrated in Fig. 10(c). As seen, there is initially a slight increase in the frequency of oscillation before the occurrence of the first saddle-node bifurcation; as the flow velocity is increased further, the oscillation frequency increases sharply, indicating increased contribution of higher modes. This is also illustrated through pipe motions at different flow velocities in Fig. 11, for the case with $\Gamma = 0.10$; as seen, second-mode flutter is dominant in Fig. 11(a) for $u = 8.23$, but as the flow velocity is increased (i.e. sub-figures (b) and (c)), the contribution of higher modes in the pipe motion increases.

The next set of figures, i.e. Figs. 12, 13, and 14, corresponds to relatively large values of Γ. More specifically, the response

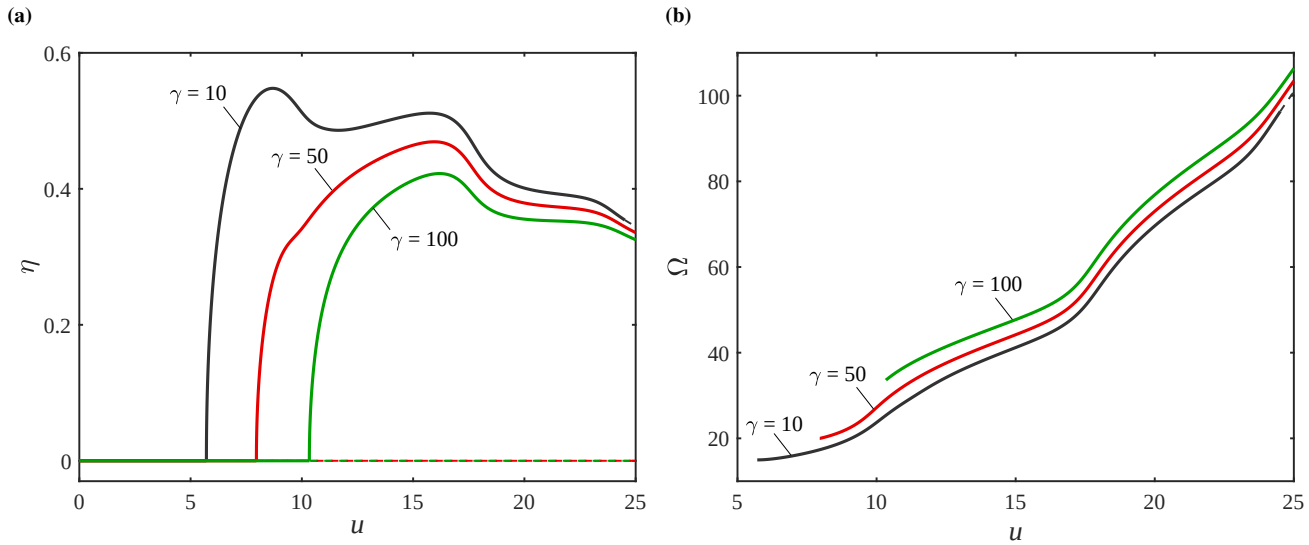

Figure 8: Bifurcation diagrams showing (a) the maximum (positive) transverse tip displacement and (b) the frequency of the transverse oscillation, obtained for a system with $\beta = 0.142$, $\Gamma = 0$ and various values of γ.

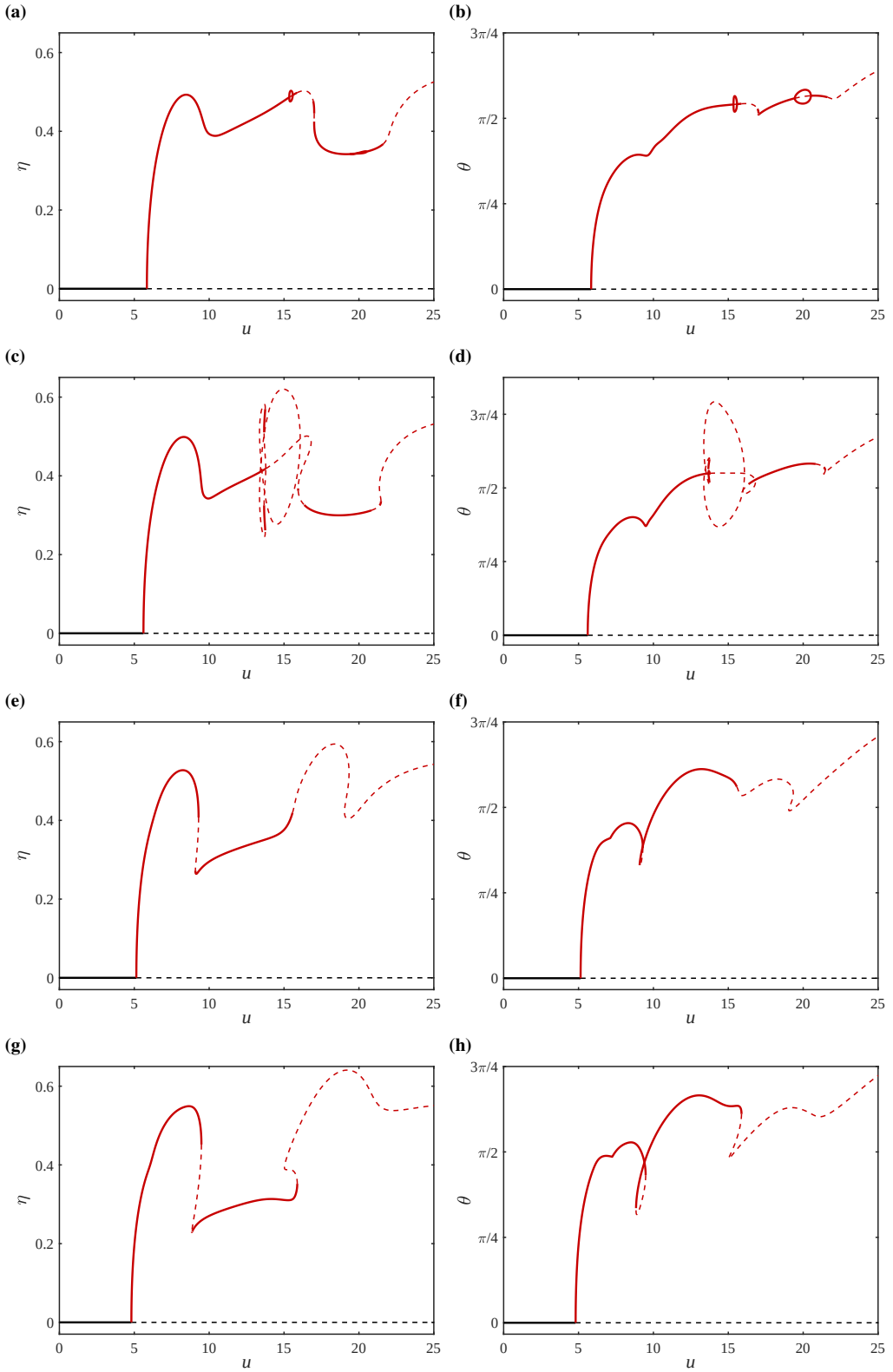

Figure 9: Bifurcation diagrams showing (left) the maximum (positive) transverse tip displacement, and (right) the maximum (positive) tip rotation angle, obtained for (a, b) $\Gamma = 0.03$, (c, d) $\Gamma = 0.05$, (e, f) $\Gamma = 0.10$, and (g, h) $\Gamma = 0.15$. [▬] Stable static solution, [▬ ▪ ▬] unstable static solution, [▬] stable periodic solution, [▬ ▪ ▬] unstable periodic solution.

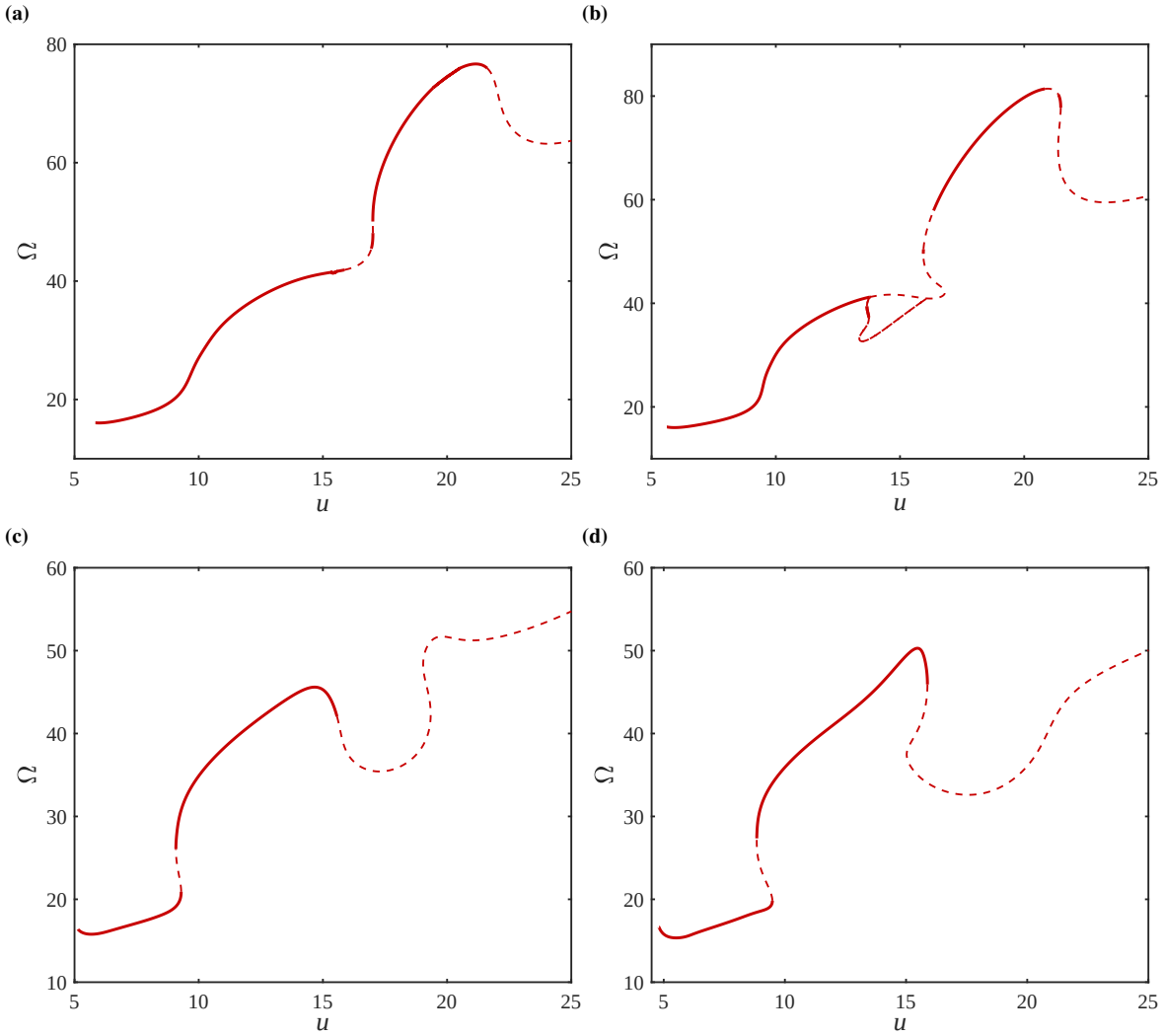

Figure 10: Frequency of pipe transverse oscillation as a function of flow velocity for (a) $\Gamma = 0.03$, (b) $\Gamma = 0.05$, (c) $\Gamma = 0.10$, and (d) $\Gamma = 0.15$.

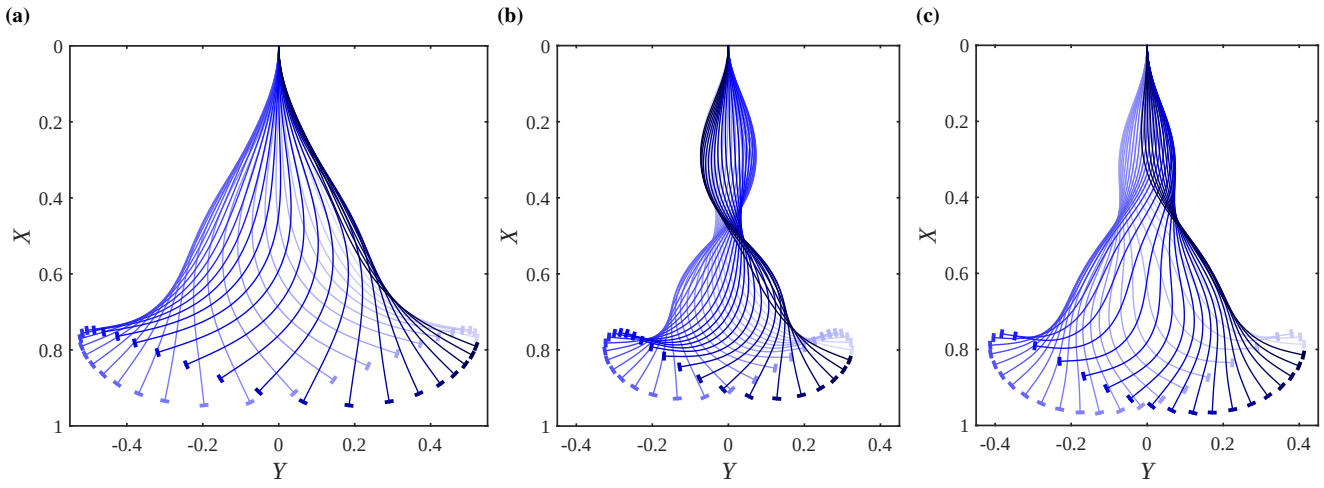

Figure 11: Shapes of the oscillating pipe of Fig. 9(e, f), i.e. with $\Gamma = 0.10$; (a) $u = 8.23$, (b) $u = 12.03$, and (c) $u = 15.56$, showing that the tip angle exceeds $\pi/2$.

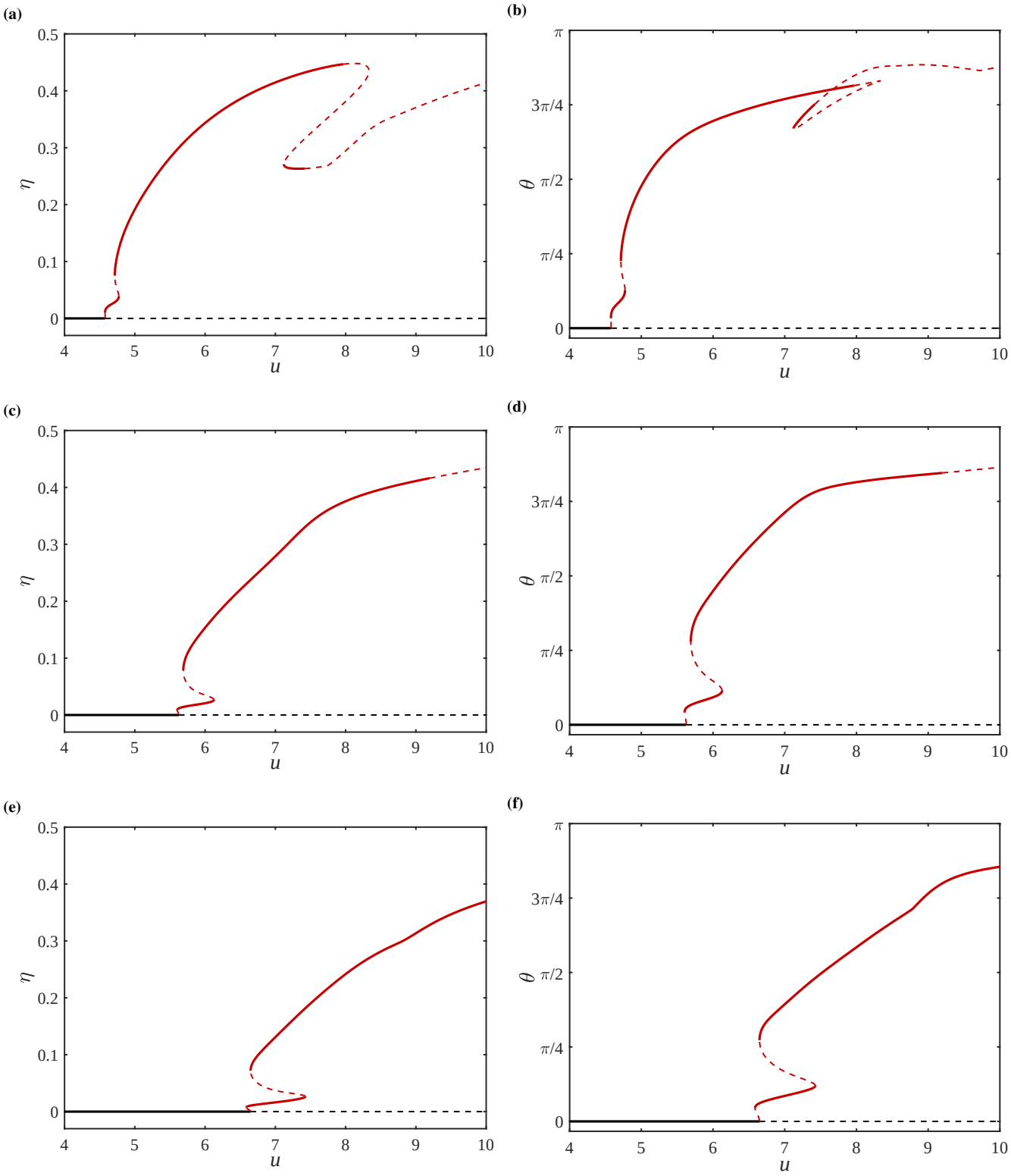

Figure 12: Bifurcation diagrams showing (left) the maximum (positive) transverse tip displacement, and (right) the maximum (positive) tip rotation angle, obtained for (a, b) $\Gamma = 1.0$, (c, d) $\Gamma = 2.0$, and (e, f) $\Gamma = 3.0$. [▬] Stable static solution, [▬ ▬] unstable static solution, [▬] stable periodic solution, [▬ ▬] unstable periodic solution.

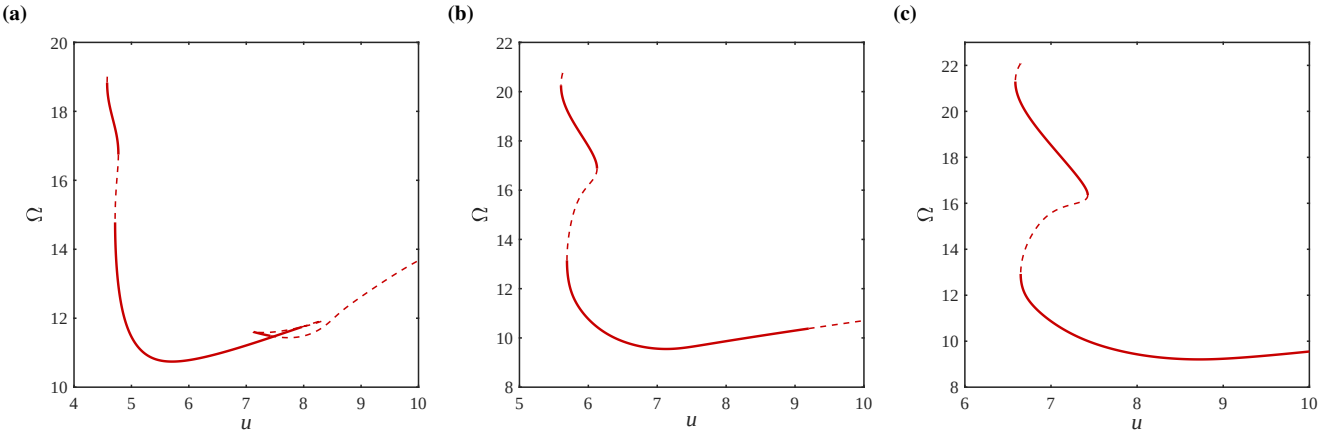

Figure 13: Frequency of pipe transverse oscillation as a function of flow velocity for (a) $\Gamma = 1.0$, (b) $\Gamma = 2.0$, and (c) $\Gamma = 3.0$.

of the fluid-conveying cantilevered pipe for relatively large values of tip mass ratio, i.e. $\Gamma = 1.0$, 2.0, and 3.0, is shown in Fig. 12, while the corresponding transverse dimensionless oscillation frequency versus flow velocity is shown in Fig. 13. The pipe motion for the case $\Gamma = 3.0$ is shown in Fig. 14.

As seen in Fig. 12, for such large values of Γ, the supercritical Hopf bifurcation is replaced by a subcritical one with S-shape response in the vicinity of the critical flow velocity, consisting of two unstable solution branches and three saddle-node bifurcations. It is seen that, contrary to the effect of smaller values of Γ, as the tip mass ratio is increased, the critical flow velocity is increased as well. Similar observations have been made by Copeland & Moon (1992) who reported measurements for large Γ. Additionally, the figure shows that, for the range of u examined here, the pipe response becomes generally simpler as Γ is increased. Furthermore, referring to Fig. 13, it is interesting to note that, unlike the case with small tip mass ratios, in this case the frequency decreases sharply with increasing u until reaching a minimum and then increases gradually. As seen, the hysteresis-type behaviour becomes stronger as the tip mass ratio is increased.

The pipe oscillation in one period for the case $\Gamma = 3.0$ is shown in Fig. 14, for three flow velocities; as seen, the pipe

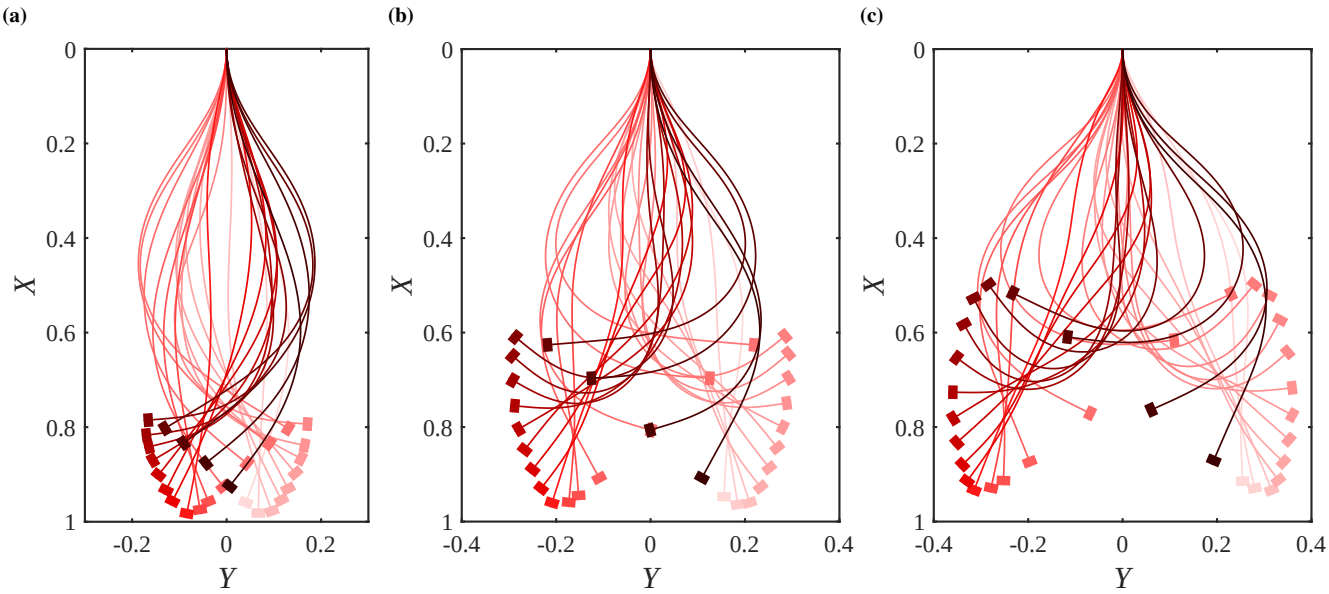

Figure 14: Shapes of the oscillating pipe of Fig. 12(e, f), i.e. $\Gamma = 3.0$; (a) $u = 7.42$ (b) $u = 8.83$, and (b) $u = 10.00$.

oscillation amplitude and its rotation over the whole pipe length grow as the flow velocity is increased. In particular, sub-figure 14(c) shows that the tip reaches angles much larger than $\pi/2$ and even close to π, which further manifests the necessity of employing an exact model for accurate prediction of the pipe motion.

It ought to be mentioned that caution must be exercised in interpreting the unstable periodic solutions obtained via the continuation technique for some flow ranges. In section 4.3, a complementary analysis is conducted to assess the global dynamics and the nature of the motion in these flow ranges.

4.3. Global dynamics

This section examines the dynamics of the pipe conveying fluid with small values of tip mass ratio via constructing the bifurcation diagrams of Poincaré sections. The trigger used for the Poincaré sections is that the tip velocity passes through zero. The reason for constructing these diagrams is that the previous bifurcation diagrams obtained via continuation analysis only provide details about stable periodic motions; in other words, the continuation method does not provide any information on nonperiodic, such as quasiperiodic and chaotic, motions. The bifurcation diagrams of Poincaré sections, on the other hand, are capable of providing motion details irrespective of the type of motion. In this section, the bifurcation diagrams are constructed for three representative values of Γ, i.e. $\Gamma = 0.05$, 0.10, and 0.15. In order to obtain the bifurcation diagrams, the discretised equations of the exact model are solved in the time domain utilising the Gear backward differentiation formula, for τ in the range [0 500]. Only the last 40% of the time histories are retained to ensure removal of any transient responses.

The bifurcation diagram for $\Gamma = 0.05$ is shown in Fig. 15. As seen, the pipe exhibits various types of motion such as periodic, period-3, quasiperiodic and chaotic motions. More specifically, the single dots in Fig. 15(a) for $u < 5.2$ (forming a straight line) represent the original position of the pipe at rest. Two dots (positive and negative) in the range $[5.2\ 13.8]$ indicate a periodic motion (period-1). The pipe undergoes a chaotic motion in a narrow range of $[13.8\ 14.2]$, associated with a wide band of dots in the bifurcation diagram. The motion of the pipe becomes dominantly period-3, followed by a wide region of periodic motion in $u \in [16.8\ 20.8]$. Finally, the motion of the pipe becomes chaotic at *circa* $u = 21.4$ after a narrow range of quasiperiodic oscillations. In order to visualize the type of motion, relevant time histories and phase-plane portraits are also presented respectively in Fig. 15(b) and (c) for $u = 14.050$, showing a random-like time trace and a dense phase-plane diagram, suggesting the existence of chaotic motion. Additionally, the details of the period-3 motion at $u = 15.025$ are shown in Fig. 15(d) and (e).

The global dynamics of the pipe with $\Gamma = 0.10$ is shown in Fig. 16. With increasing u, the pipe loses its static stability at $u = 5.61$ via a supercritical Hopf bifurcation leading to a period-1 oscillation around the origin. In the range $u \in [17.05\ 19.23]$, the motion becomes stable quasiperiodic with two incommensurate frequencies; sample results are shown in subfigures (b) and (c) for $u = 18.025$. The pipe undergoes periodic motion at $u = 19.23$, followed by period-2 oscillations at $u = 20.8$; finally, chaotic oscillations arise for higher flow velocities.

Similar qualitative behaviour can be seen for the case with $\Gamma = 0.15$ in Fig. 17. It is found that secondary bifurcations leading to periodic, period-n, and chaotic oscillations emanate at flow velocities beyond the first Hopf bifurcation. However, in contrast to lower values of Γ, the pipe does not return to period-1 motion at high flow velocities. The chaotic motion is associated with erratic oscillations taking place mainly around the undeflected equilibrium with varying amplitude and period. Looking at the phase-plane plot, it reflects the existence of an overriding rather strong periodic component in the motion. The power spectral density (PSD) is quite dense, yet showing that one dominant frequency survives. Although the probability

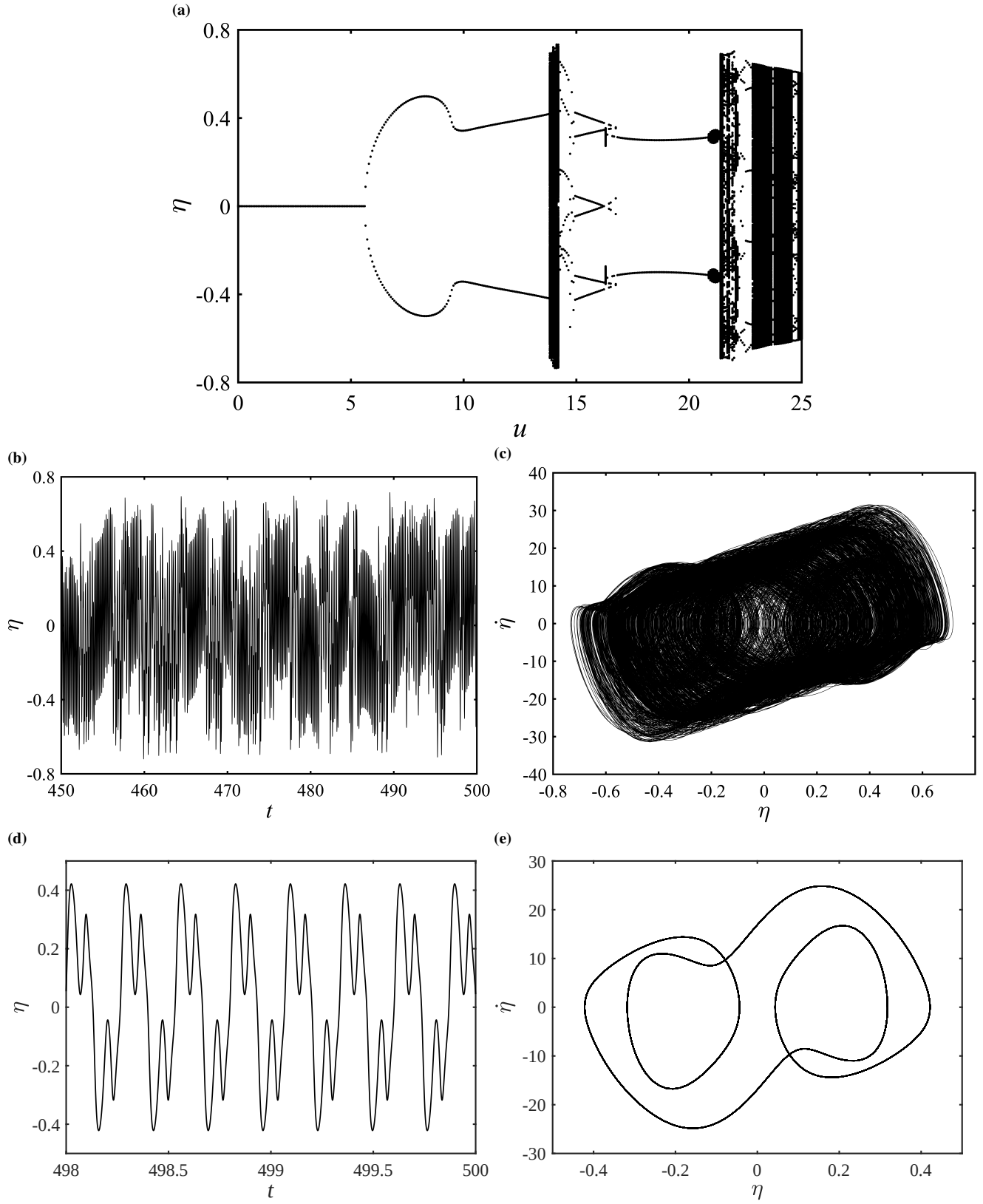

Figure 15: (a) Bifurcation diagram showing the maximum and minimum transverse tip displacement, obtained for $\beta = 0.142$, $\gamma = 18.9$, and $\Gamma = 0.05$; (b) time history and (c) phase-plane plots of response at $u = 14.050$, indicating a chaotic motion; (d) time history and (e) phase-plane plots of response at $u = 15.025$, indicating a period-3 motion.

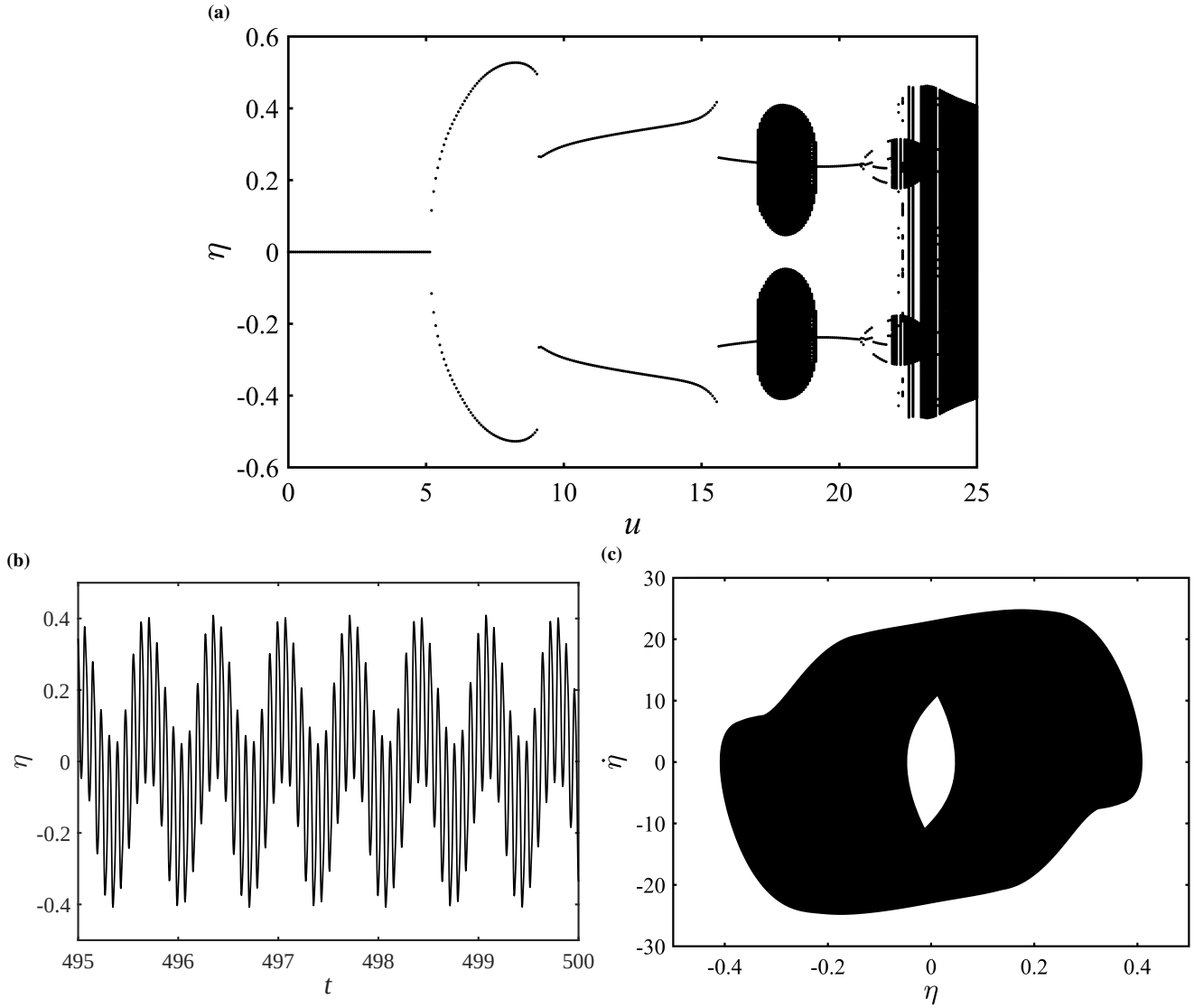

Figure 16: (a) Bifurcation diagram showing the maximum and minimum transverse tip displacement, obtained for $\beta = 0.142$, $\gamma = 18.9$, and $\Gamma = 0.10$; (b) time history and (c) phase-plane plots of response at $u = 18.025$, indicating a quasi-periodic motion.

density function (PDF) does not have a Gaussian distribution and it is still double-masted, it possesses a suspension-bridge shape filling up between the two peaks, indicating the mostly visited locations by the pipe tip during the motion. All are characteristics of chaotic oscillation, albeit with a surviving periodic component.

It ought to be mentioned that in order to refer to the motion in this flow regime as categorically “chaotic", a more rigorous sensitivity analysis of dependence of the system response on initial conditions by virtue of the Lyapunov stability definition is required.

5. Concluding remarks

In this study, the nonlinear large-amplitude dynamics of a hanging pipe has been investigated utilising a geometrically exact model. More specifically, a highly accurate model for centreline rotation of a fluid-conveying cantilevered pipe was developed utilising Hamilton’s principle while keeping all the terms geometrically exact. The distinguishing feature of such an exact model, compared to other nonlinear truncated models, is that it allows for accurate analysis of the pipe dynamics even at

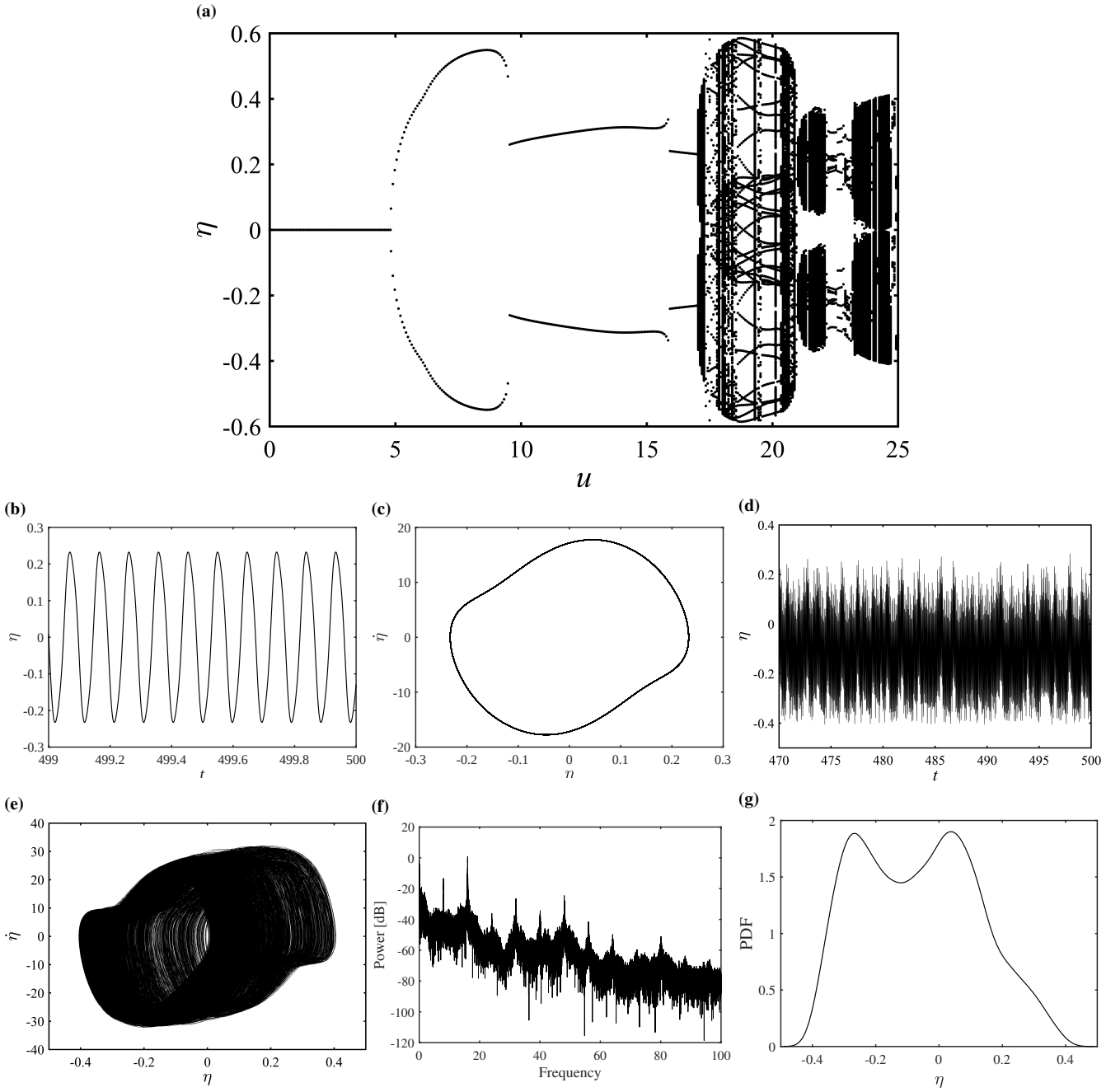

Figure 17: (a) Bifurcation diagram showing the maximum and minimum transverse tip displacement, obtained for $\beta = 0.142$, $\gamma = 18.9$, and $\Gamma = 0.15$; (b) time history and (c) phase-plane plots of response at $u = 16.825$, indicating a periodic motion; (d) time history, (e) phase-plane, (f) power spectral density, and (g) probability density function plots of response at $u = 24.400$, indicating a chaotic motion.

extremely large rotations and oscillation amplitudes. A high-dimensional modal decomposition was conducted via the Galerkin scheme to obtain the discretised nonlinear equations, which were then solved via use of a continuation technique as well as a time integration method.

A convergence analysis demonstrated that low-dimensional models (i.e. 2-, 3-, and 4-dof ones) do not yield reliable results and they tend to diverge at relatively large flow velocities, especially in the presence of a tip mass. It was shown that, at

least 8 modes must be retained in the discretisation procedure, and that a 10-dof model (the one used in this study) ensures reliable predictions even at very large flow velocities or large tip mass ratios. Additionally, comparisons between the proposed exact model and a nonlinear third-order model revealed that the deviation between the two starts almost immediately after the occurrence of the Hopf bifurcation. Also, the discrepancy between the two models is exacerbated with increasing flow velocity and/or the tip mass ratio. These results indicate that it is essential to use an exact model when analysing dynamics of a fluid-conveying cantilevered pipe which may involve large-amplitude oscillations and extremely large rotations.

The effects of some of the key parameters affecting the system dynamics were explored. It was shown that the dynamics of cantilevered pipe with an end mass displays a number of bifurcations as the flow velocity is varied. Quasiperiodic and chaotic motions were observed for the range of tip mass ratios investigated. Additionally, possible by means of the present model is the prediction of changes in flutter amplitudes with increasing β or γ due to changes in the modal shape of oscillations, and how these vary with flow velocity, as well as many other quantitative and qualitative post-bifurcation facets of the system dynamics.

It is emphasised that the high-dimensional exact model proposed in this study enabled us, for the first time, to reveal the global dynamics of pipes with a tip mass at high flow velocities. Fresh experiments with cantilevered pipes at high flow velocities are required to validate the predictions of the proposed model.

CRediT authorship contribution statement

Hamed Farokhi: Conceptualization, Methodology, Software, Validation, Formal analysis, Investigation, Writing - original draft, Writing - review & editing, Visualization. **Mohammad Tavallaeinejad**: Conceptualization, Software, Investigation, Writing - original draft, Writing - review & editing, Visualization. **Michael P. Païdoussis**: Conceptualization, Investigation, Writing - original draft, Writing - review & editing.

References

BAJAJ, A. K. & SETHNA, P. R. 1984 Flow induced bifurcations to three-dimensional oscillatory motions in continuous tubes. *SIAM Journal on Applied Mathematics* **44** (2), 270–286.

BAJAJ, A. K. , SETHNA, P. R. & LUNDGREN, T. S. 1980 Hopf bifurcation phenomena in tubes carrying a fluid. *SIAM Journal on Applied Mathematics* **39** (2), 213–230.

BENJAMIN, T. B. 1961*a* Dynamics of a system of articulated pipes conveying fluid - II. Experiments. *Proceedings of the Royal Society of London. Series A. Mathematical and Physical Sciences* **A261** (1307), 487–499.

BENJAMIN, T. B. 1961*b* Dynamics of a system of articulated pipes conveying fluid-I. Theory. *Proceedings of the Royal Society of London. Series A. Mathematical and Physical Sciences* **A261** (1307), 457–486.

BOURRIÈRES, F.-J. 1939 *Sur un phénomène d'oscillation auto-entretenue en mécanique des fluides réels. Publications scientifiques et techniques du Ministère de l'Air No.147*. E. Blondel La Rougery, Gauthier-Villars.

COPELAND, G. & MOON, F. 1992 Chaotic flow-induced vibration of a flexible tube with end mass. *Journal of Fluids and Structures* **6** (6), 705–718.

DOARÉ, O. & DE LANGRE, E. 2002*a* The flow-induced instability of long hanging pipes. *European Journal of Mechanics - A/Solids* **21** (5), 857 – 867.

DOARÉ, O. & DE LANGRE, E. 2002*b* Local and global instability of fluid-conveying pipes on elastic foundations. *Journal of Fluids and Structures* **16** (1), 1–14.

EBRAHIMI-MAMAGHANI, A. , SOTUDEH-GHAREBAGH, R. , ZARGHAMI, R. & MOSTOUFI, N. 2019 Dynamics of two-phase flow in vertical pipes. *Journal of Fluids and Structures* **87**, 150 – 173.

GHAYESH, M. H. & PAÏDOUSSIS, M. P. 2010 Three-dimensional dynamics of a cantilevered pipe conveying fluid, additionally supported by an intermediate spring array. *International Journal of Non-Linear Mechanics* **45** (5), 507–524.

GREENWALD, A. S. & DUGUNDJI, J. 1967 Static and dynamic instabilities of a propellant line. *Tech. Rep.*. Massachusetts Institute of Technology Aeroelastic and Structures Research Laboratory, Report: AFOSR 67–1395.

GREGORY, R. W. & PAÏDOUSSIS, M. P. 1966*a* Unstable oscillation of tubular cantilevers conveying fluid. i. theory. *Proceedings of the Royal Society of London. Series A. Mathematical and Physical Sciences* **293** (1435), 512–527.

GREGORY, R. W. & PAÏDOUSSIS, M. P. 1966*b* Unstable oscillation of tubular cantilevers conveying fluid. ii. experiments. *Proceedings of the Royal Society of London. Series A. Mathematical and Physical Sciences* **293** (1435), 528–542.

GUO, C. , ZHANG, C. & PAÏDOUSSIS, M. 2010 Modification of equation of motion of fluid-conveying pipe for laminar and turbulent flow profiles. *Journal of Fluids and Structures* **26** (5), 793–803.

IBRAHIM, R. A. 2010 Overview of mechanics of pipes conveying fluids—Part I: Fundamental studies. *ASME Journal of Pressure Vessel Technology* **132** (3), 1–32.

IBRAHIM, R. A. 2011 Mechanics of pipes conveying fluids—Part II: applications and fluidelastic problems. *ASME Journal of Pressure Vessel Technology* **133** (2), 1–30.

KHEIRI, M. 2020 Nonlinear dynamics of imperfectly-supported pipes conveying fluid. *Journal of Fluids and Structures* **93**, 102850.

KUIPER, G. L. & METRIKINE, A. V. 2005 Dynamic stability of a submerged, free-hanging riser conveying fluid. *Journal of Sound and Vibration* **280** (3-5), 1051–1065.

MODARRES-SADEGHI, Y. , PAÏDOUSSIS, M. P. & SEMLER, C. 2008 Three-dimensional oscillations of a cantilever pipe conveying fluid. *International Journal of Non-Linear Mechanics* **43** (1), 18 – 25.

MODARRES-SADEGHI, Y. , SEMLER, C. , WADHAM-GAGNON, M. & PAÏDOUSSIS, M. P. 2007 Dynamics of cantilevered pipes conveying fluid. Part 3: Three-dimensional dynamics in the presence of an end-mass. *Journal of Fluids and Structures* **23** (4), 589–603.

MOHMMED, A. O. , AL-KAYIEM, H. H. , OSMAN, A. & SABIR, O. 2020 One-way coupled fluid–structure interaction of gas–liquid slug flow in a horizontal pipe: Experiments and simulations. *Journal of Fluids and Structures* **97**, 103083.

MONETTE, C. & PETTIGREW, M. J. 2004 Fluidelastic instability of flexible tubes subjected to two-phase internal flow. *Journal of Fluids and Structures* **19** (7), 943–956.

PAÏDOUSSIS, M. , SEMLER, C. & WADHAM-GAGNON, M. 2005 A reappraisal of why aspirating pipes do not flutter at infinitesimal flow. *Journal of Fluids and Structures* **20** (1), 147–156.

PAÏDOUSSIS, M. P. 1963 Oscillations of liquid-filled flexible tubes. PhD thesis, University of Cambridge, U.K.

PAÏDOUSSIS, M. P. 1970 Dynamics of tubular cantilevers conveying fluid. *Journal of Mechanical Engineering Science* **12** (2), 85–103.

PAÏDOUSSIS, M. P. 2014 *Fluid-Structure Interactions: Slender Structures and Axial Flow. Volume 1, 2nd edition*. Oxford: Academic Press.

PAÏDOUSSIS, M. P. & ISSID, N. T. 1974 Dynamic stability of pipes conveying fluid. *Journal of Sound and Vibration* **33** (3), 267–294.

PAÏDOUSSIS, M. P. & LI, G. X. 1993 Pipes conveying fluid: a model dynamical problem. *Journal of Fluids and Structures* **7** (2), 137–204.

PAÏDOUSSIS, M. P. & LUU, T. P. 1985 Dynamics of a pipe aspirating fluid such as might be used in ocean mining. *ASME Journal of Energy Resources Technology* **107**, 250–255.

PAÏDOUSSIS, M. P. & SEMLER, C. 1993 Nonlinear dynamics of a fluid-conveying cantilevered pipe with an intermediate spring support. *Journal of Fluids and Structures* **7** (3), 269–298.

PAÏDOUSSIS, M. P. & SEMLER, C. 1998 Non-linear dynamics of a fluid-conveying cantilevered pipe with a small mass attached at the free end. *International Journal of Non-Linear Mechanics* **33** (1), 15–32.

PAÏDOUSSIS, M. P. , SEMLER, C. , WADHAM-GAGNON, M. & SAAID, S. 2007 Dynamics of cantilevered pipes conveying fluid. Part 2: Dynamics of the system with intermediate spring support. *Journal of Fluids and Structures* **23** (4), 569–587.

PAÏDOUSSIS, M. P. & SUNDARARAJAN, C. 1975 Parametric and combination resonances of a pipe conveying pulsating fluid. *Journal ofApplied Mechanics* **42**, 780–784.

PAÏDOUSSIS, M. P. & TÉTREAULT-FRIEND, M. 2009 Aspirating cantilevers and reverse sprinklers. *American Journal of Physics* **77** (4), 349–353.

PAI, P. F. 2014 Problems in geometrically exact modeling of highly flexible beams. *Thin-Walled Structures* **76**, 65–76.

RINALDI, S. & PAÏDOUSSIS, M. P. 2010 Dynamics of a cantilevered pipe discharging fluid, fitted with a stabilizing end-piece. *Journal of Fluids and Structures* **26** (3), 517–525.

SADEGHI-GOUGHARI, M. , JEON, S. & KWON, H.-J. 2020 Fluid structure interaction of cantilever micro and nanotubes conveying magnetic fluid with small size effects under a transverse magnetic field. *Journal of Fluids and Structures* **94**, 102951.

SAZESH, S. & SHAMS, S. 2019 Vibration analysis of cantilever pipe conveying fluid under distributed random excitation. *Journal of Fluids and Structures* **87**, 84 – 101.

SEMLER, C. , ALIGHANBARI, H. & PAÏDOUSSIS, M. P. 1998 A physical explanation of the destabilizing effect of damping. *Journal of Applied Mechanics* **65**, 642–648.

SIMO, J. C. & VU-QUOC, L. 1988 On the dynamics in space of rods undergoing large motions—a geometrically exact approach. *Computer Methods in Applied Mechanics and Engineering* **66** (2), 125–161.

STEINDL, A. & TROGER, H. 1995 Nonlinear three-dimensional oscillations of elastically constrained fluid conveying viscoelastic tubes with perfect and broken o (2)-symmetry. *Nonlinear Dynamics* **7** (2), 165–193.

TANG, S. & SWEETMAN, B. 2021 A geometrically-exact momentum-based nonlinear theory for pipes conveying fluid. *Journal of Fluids and Structures* **100**, 103190.

TAVALLAEINEJAD, M. , PAÏDOUSSIS, M. P. & LEGRAND, M. 2018 Nonlinear static response of low-aspect-ratio inverted flags subjected to a steady flow. *Journal of Fluids and Structures* **83**, 413 – 428.

TAVALLAEINEJAD, M. , PAÏDOUSSIS, M. P. , LEGRAND, M. & KHEIRI, M. 2020 Instability and the post-critical behaviour of two-dimensional inverted flags in axial flow. *Journal of Fluid Mechanics* **890**, A14.

WADHAM-GAGNON, M. , PAÏDOUSSIS, M. P. & SEMLER, C. 2007 Dynamics of cantilevered pipes conveying fluid. Part 1: Nonlinear equations of three-dimensional motion. *Journal of Fluids and Structures* **23** (4), 545–567.

ZHENG, D. , WANG, S. , LIU, B. & FAN, S. 2016 Theoretical analysis and experimental study of coriolis mass flow sensor sensitivity. *Journal of Fluids and Structures* **65**, 295–312.